Molecular Biology of the Cell
Vol. 21, 1810–1824, June 1, 2010

Involvement of the Cytoskeleton in Controlling Leading-Edge Function during Chemotaxis

Susan Lee,* Zhouxin Shen,* Douglas N. Robinson,† Steven Briggs,* and Richard A. Firtel*

*Section of Cell and Developmental Biology, Division of Biological Sciences, University of California, San Diego, La Jolla, CA 92093-0380 and †Departments of Cell Biology, Pharmacology and Molecular Sciences, and Chemical and Biomolecular Engineering, Center for Cell Dynamics and NanoBioMed, Johns Hopkins School of Medicine, Baltimore, MD 21205

Submitted January 6, 2010; Revised March 16, 2010; Accepted March 31, 2010
Monitoring Editor: Peter Van Haastert

In response to directional stimulation by a chemoattractant, cells rapidly activate a series of signaling pathways at the site closest to the chemoattractant source that leads to F-actin polymerization, pseudopod formation, and directional movement up the gradient. Ras proteins are major regulators of chemotaxis in *Dictyostelium*; they are activated at the leading edge, are required for chemoattractant-mediated activation of PI3K and TORC2, and are one of the most rapid responders, with activity peaking at ~3 s after stimulation. We demonstrate that in myosin II (MyoII) null cells, Ras activation is highly extended and is not restricted to the site closest to the chemoattractant source. This causes elevated, extended, and spatially misregulated activation of PI3K and TORC2 and their effectors Akt/PKB and PKBR1, as well as elevated F-actin polymerization. We further demonstrate that disruption of specific IQGAP/cortexillin complexes, which also regulate cortical mechanics, causes extended activation of PI3K and Akt/PKB but not Ras activation. Our findings suggest that MyoII and IQGAP/cortexillin play key roles in spatially and temporally regulating leading-edge activity and, through this, the ability of cells to restrict the site of pseudopod formation.

INTRODUCTION

The ability of amoeboid cells such as *Dictyostelium* cells, neutrophils, or macrophages to sense and respond to directional chemical cues and move up a chemoattractant gradient is central to a wide range of cellular processes (Jin *et al.*, 2008; Sallusto and Baggiolini, 2008). Cells must efficiently integrate multiple signaling responses to coordinate F-actin–mediated protrusion at the leading edge and actomyosin contraction at the cell's posterior (Kehrl, 2006; Van Haastert and Veltman, 2007; Janetopoulos and Firtel, 2008). In *Dictyostelium*, Ras is required for efficient directional sensing and chemotaxis, lies upstream of and regulates PI3K (phosphatidylinositol 3-kinase) and TOR Complex 2 (TORC2), and is activated at the leading edge (Lee *et al.*, 1999, 2005; Sasaki *et al.*, 2004, 2007; Bolourani *et al.*, 2006; Kae *et al.*, 2007; Van Haastert and Veltman, 2007). Other pathways (Rap1 and guanylyl cyclase), which have been linked to myosin II (MyoII) regulation, are also activated at the leading edge. Rap1 functions, in part, to disassemble MyoII filaments at the leading edge through the activation of the Ser/Thr kinase Phg2, whereas cGMP, the product of guanylyl cyclase, mediates MyoII assembly and function in the cell's posterior (Rebstein *et al.*, 1997; Gebbie *et al.*, 2004; Bosgraaf and Van Haastert, 2006; Kortholt *et al.*, 2006; Jeon *et al.*, 2007; Kortholt and Van Haastert, 2008). Of these leading-edge pathways, Ras activation is the earliest known response downstream from the receptor and heterotrimeric G proteins in *Dictyostelium* with activity peaking at ~3 s after stimulation (Sasaki *et al.*, 2004).

When cells are given a uniform (global) stimulation of chemoattractant, pathways that regulate the formation of the leading edge are rapidly and uniformly activated along the cell's cortex. In both *Dictyostelium* and neutrophils, these pathways are amplified through positive feedback loops that involve F-actin, causing signal amplification and stabilization of the leading edge, which are critical for cells to move up shallow, weak chemoattractant gradients (Rubin and Ravid, 2002; Sasaki *et al.*, 2004; Van Keymeulen *et al.*, 2006; Brandman and Meyer, 2008). In concert with these responses, cortical MyoII is disassembled through phosphorylation contemporaneously with F-actin polymerization (Moores *et al.*, 1996; de la Roche and Cote, 2001; Funamoto *et al.*, 2002; Iijima and Devreotes, 2002). In chemotaxing cells, cortical MyoII is spatially distributed along the lateral sides and backs of cells, areas in which leading-edge signaling pathways are normally not activated, where it provides cortical tension (rigidity) and contraction of the posterior during cell movement (Wessels *et al.*, 1988; Egelhoff *et al.*, 1996; Stites *et al.*, 1998; Xu *et al.*, 2001; Laevsky and Knecht, 2003; Reichl *et al.*, 2008).

Leading-edge (front) and trailing edge (back) responses are also spatially restricted and balanced. In neutrophils, pathways regulated by the heterotrimeric G protein G_i control leading-edge responses, including PI3K, Rac, and F-actin polymerization, whereas $G_{11/12}$, regulates RhoA, MyoII assembly, and contraction in the posterior (Weiner *et al.*,

This article was published online ahead of print in *MBoC in Press* (http://www.molbiolcell.org/cgi/doi/10.1091/mbc.E10–01–0009) on April 7, 2010.

Address correspondence to: Richard A. Firtel (rafirtel@ucsd.edu).

Abbreviations used: ctx, cortexillin; LatB, latrunculin B; *mhcA*$^-$, myosin II null; MHCK, myosin II heavy-chain kinase; MyoII, myosin II; PI3K, phosphatidylinositol 3-kinase; TORC2, TOR complex 2.

2002; Li *et al.*, 2003, 2005; Van Keymeulen *et al.*, 2006). Inhibition of one of these pathways causes up-regulation of the other. *Dictyostelium* cells lacking MyoII (*mhcA*$^-$ cells) are unable to inhibit lateral pseudopodia and produce them simultaneously along the lateral sides of cells, in addition to being defective in contracting their posteriors and often exhibiting decreased polarity (Wessels *et al.*, 1988). Mammalian cells in which RhoA activity or the activity of the Rho kinase (ROCK) is inhibited exhibit similar phenotypes (Xu *et al.*, 2003; Wu *et al.*, 2009). PTEN, a negative regulator of the PI3K pathway, localizes to the sides and posterior of chemotaxing cells and is thought to play a role in restricting phosphatidylinositol (3,4,5)-triphosphate [PI(3,4,5)P_3] accumulation to the leading edge (Funamoto *et al.*, 2002; Iijima and Devreotes, 2002; Zhang *et al.*, 2008). The RasGAP Dd-NF1 also plays a key part in temporally controlling RasG and downstream PI3K signaling, is required for establishing a defined leading edge, and is important for directional sensing.

Although some progress has been made, the mechanisms that restrict the activation of leading-edge pathways to the front of the cell, and thereby inhibit pathways from being activated along the lateral sides and posterior, are still not well understood. The observations that cells lacking MyoII (*mhcA*$^-$ cells) are unable to properly inhibit the formation of lateral pseudopodia suggested the possibility that components of the cytoskeleton may be important negative regulators of leading-edge function. To investigate this possibility, we examined the spatial and temporal control of Ras and PI3K signaling in cells in which MyoII function is either lost or altered and in cells lacking the IQGAP/cortexillin complex, which plays an important role as an F-actin cross-linker and in regulating cortical mechanics. IQGAPs are found in all eukaryotes and are required for cytokinesis in *Dictyostelium*, *Saccharomyces cerevisiae*, and *Schizosaccharomyces pombe*. IQGAPs contain a conserved a RasGAP-related Rac1-GTP–binding domain near their C-terminus, a C-terminal effector-binding domain, and an N-terminus of varying length (Adachi *et al.*, 1997; Lee *et al.*, 1997; Eng *et al.*, 1998; Faix *et al.*, 1998; Osman and Cerione, 1998; Briggs and Sacks, 2003; Bensenor *et al.*, 2007; Brandt and Grosse, 2007). In *Dictyostelium*, activated Rac1 (Rac1-GTP) binding to DdIQGAP1 (DGAP1) leads to the recruitment of a dimer of the F-actin bundling protein cortexillin I (ctxI) to a Rac1-GTP/IQGAP1/ctxI complex at the cleavage furrow during cytokinesis and is involved with the control of MyoII localization (Faix *et al.*, 1998, 2001; Ren *et al.*, 2009). DdIQGAP1 has also been linked to cell motility and morphogenesis; the expression level of IQGAP1, but not DdIQGAP2 (GAPA), has been correlated to the rate of cell motility.

We have found that MyoII and IQGAP/ctx play distinct and independent roles in regulating leading-edge function. MyoII is important for controlling Ras activity, and cells lacking MyoII have greatly extended Ras activation and exhibit Ras and PI3K activation randomly along the cell cortex, which we suggest is responsible for the adventitious formation of lateral pseudopodia. In contrast, cells lacking specific combinations of IQGAPs and ctxs exhibit normal activation of Ras but high and extended activation of PI3K and elevated F-actin levels. These studies provide new evidence that MyoII and IQGAP/ctx are important in restricting at least some leading-edge pathways to the site on the cortex closest to the chemoattractant source.

We have investigated the spatial and temporal control of two key leading-edge pathways, Ras and PI3K. Our findings support a role for MyoII in regulating the spatiotemporal control of Ras signaling and for IQGAP/ctx in inhibiting and spatially restricting the extent of activation of PI3K but not Ras, suggesting that different F-actin regulators play distinct roles in controlling leading-edge function.

MATERIALS AND METHODS

F-Actin Polymerization and MyoII Assembly

Cells were starved for 2 h, pulsed with 100 nM cAMP for 5 h, and treated with 1 mM caffeine for 30 min before stimulation with 100 mM cAMP. Cytoskeletal proteins were isolated as proteins insoluble in the detergent Triton X-100 as described previously (Meili *et al.*, 1999; Steimle *et al.*, 2001). The protein pellets were dissolved by being boiled in 2× SDS-PAGE sample buffer, run on 8% acrylamide gels, and stained with Coomassie blue. Protein bands were scanned, and changes in actin and MyoII content were quantified using Image Gauge software (Fuji, Stamford, CT). All experiments were repeated at least three times on separate days with internal wild-type cells assayed contemporaneously to provide an internal reference.

cAMP Stimulation of Dictyostelium *Cells*

To produce aggregation-competent cells, log-phase vegetative cells were washed twice with 12 mM Na/K phosphate buffer and resuspended to a density of 7×10^6 cells/ml in Na/K phosphate buffer (Insall *et al.*, 1994). Cells were pulsed with 30 nM cAMP at 6-min intervals for 5 h. The cells were spun down and resuspended to 2×10^7 cells/ml in Na/K phosphate buffer, pH 6.2. The cells were stimulated with 1 μM cAMP, and time points were taken as indicated. All experiments were repeated at least three times on separate days with internal wild-type cells assayed contemporaneously to provide an internal reference.

Akt/Protein Kinase B Kinase Activity Assay

Assays for Akt/protein kinase B (PKB) and PKBR1 were performed as described previously (Meili *et al.*, 1999, 2000). We determined the relative activity of Akt/PKB after cAMP stimulation using H2B (Histone 2B) as a substrate. We measured ^{32}P phosphate incorporation using a Typhoon 9400 phosphorimager (GE Healthcare, Piscataway, NJ). All experiments were repeated at least three times on separate days with internal wild-type cells assayed contemporaneously to provide an internal reference.

Chemotaxis Assay

We performed the chemotaxis analysis as described previously using cAMP-stimulated cells (Funamoto *et al.*, 2001). Eppendorf "femtotip" micropipettes containing 150 mM cAMP were used without applied pressure for the chemotaxis assays. We did the computer analysis by using DIAS software (Soll Technologies, Iowa City, IA; Wessels *et al.*, 1988). At least five cells were analyzed for at least three separate movies taken on separate days, and the chemotaxis assays were performed at least three times on separate days.

Phalloidin Staining

We performed phalloidin staining as described previously (Chung *et al.*, 2000). Pulsed cells were spotted on a coverslip and let stand for 10 min. Cells were fixed with 3.7% formaldehyde for 10 min and then permeablized with 0.2% Triton X-100 for 1 min. We stained the cells with TRITC-labeled phalloidin containing 0.1% bovine serum albumin (BSA) and 0.2% Tween 20 for 1 h. After washing, we observed the cells with a 63× oil immersion lens on a Leica microscope (Deerfield, IL).

Ras Pulldown Assay

Ras pulldown assays were done as described previously (Sasaki *et al.*, 2004). The cell extract was incubated with 10 μg of glutathione *S*-transferase (GST)-RBD (Rac-binding domain) on glutathione-agarose beads at 4°C for 30 min in the presence of 5 mg/ml BSA. We washed the beads three times. Ras proteins were separated on a 12% SDS-PAGE gel and immunoblotted with anti-Pan-Ras antibody. All experiments were repeated at least three times on separate days with internal wild-type cells assayed contemporaneously to provide an internal reference.

Strains

The ctxI, ctxII, and ctxI/II null strains were obtained from the *Dictyostelium* stock center. The mhcA$^-$ strain was from the stock center and another was also created in our laboratory. The phenotypes of the two strains were indistinguishable. The constructs and Southern blots of the newly created strains are shown in Supplemental Figure 6. Double knockouts were made by sequential use of Bsr and Hygro cassettes at the same insertion point in the knockout construct.

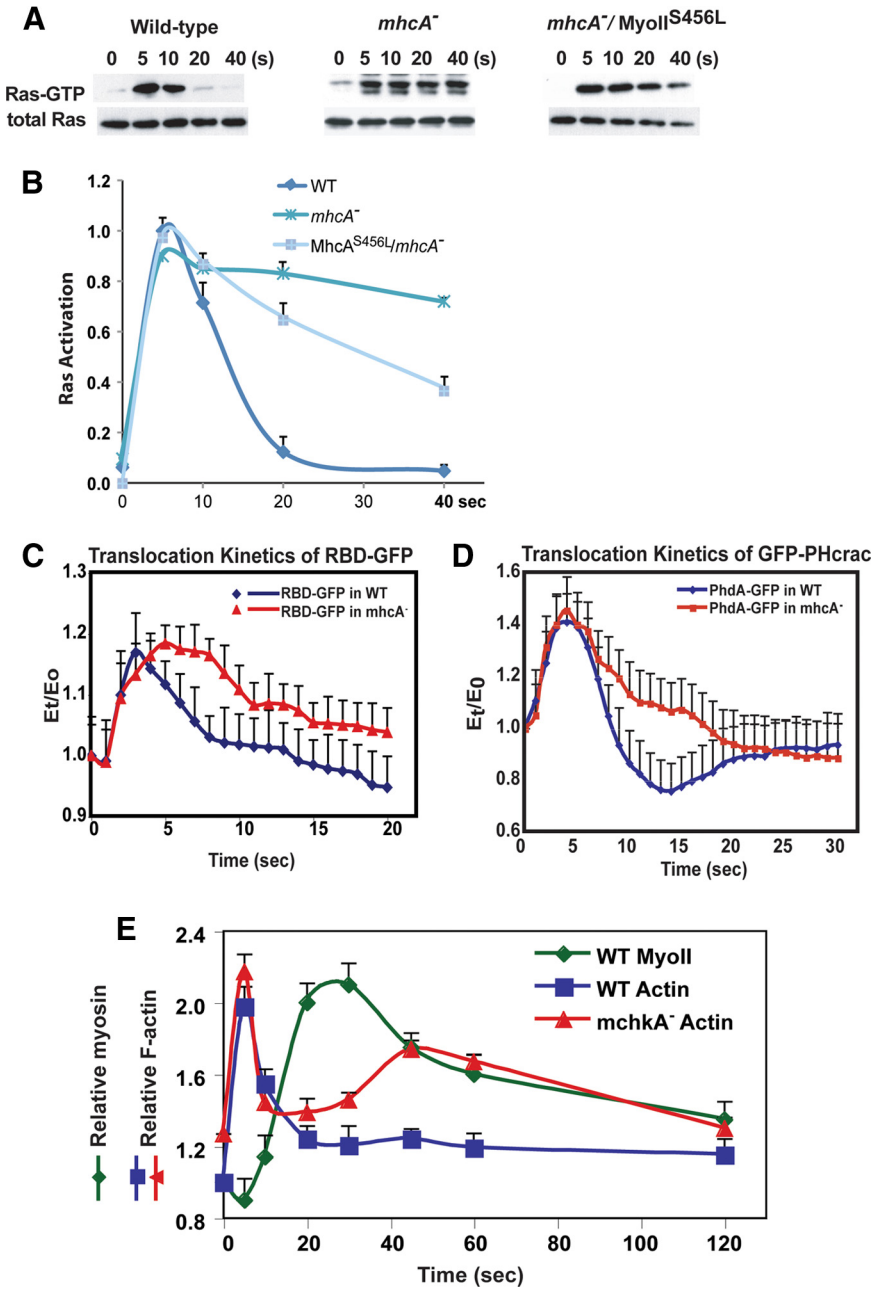

Figure 1. Regulation of Ras by MyoII. (A) Ras activation in wild-type, *mhcA*$^-$, and *mhcA*$^-$/MyoII^{S456L} cells. (B) Comparative quantitation of Ras activation (see *Materials and Methods*). Maximum value of wild-type cells is taken as 1.0. (C) Translocation kinetics of RBD-GFP in KAx-3 and *mhcA*$^-$ cells before and after stimulation. (D) Translocation kinetics of PhdA-GFP in KAx-3 and *mhcA*$^-$ cells before and after cAMP stimulation. (E) Kinetics of F-actin polymerization of KAx3 and *mhcA*$^-$ cells, and MyoII assembly of KAx-3 in the Triton-insoluble, cytoskeleton fraction.

RESULTS

Activation of Ras and Ras Effector Pathways Is Extended and Misregulated in mhcA$^-$ *cells*

One hypothesis to explain the increase in lateral pseudopodia and the elevated F-actin response is that *mhcA*$^-$ cells might be unable to restrict leading-edge signaling pathways to the site of the cell closest to the chemoattractant source, resulting in the simultaneous activation of these responses at many sites along the cell's cortex, which then lead to the formation of multiple F-actin protrusions. To test this hypothesis, we examined the kinetics and extent of activation of the Ras and PI3K pathways known to regulate F-actin polymerization in *Dictyostelium* (Chen *et al.*, 2003; Sasaki *et al.*, 2004, 2007; Zhang *et al.*, 2008). Figure 1, A and B, depicts the analysis of Ras activation using a pulldown assay, which is extended in *mhcA*$^-$ cells compared with that in wild-type cells (Table 1). Both strains exhibit a rapid increase in Ras-GTP levels upon chemoattractant stimulation, when wild-type cells rapidly decrease to basal levels by the 20-s time point, as described previously (Sasaki *et al.*, 2004). In contrast, in *mhcA*$^-$ cells, Ras-GTP levels remain elevated for an extended time.

We then studied the extent and kinetics of Ras activation in vivo using the real-time Ras-GTP reporter green fluorescent protein (GFP)-RBD, which binds to Ras-GTP and translocates to the plasma membrane in response to Ras activation, where it binds to Ras-GTP. Figure 1C shows the quantitation of these assays. Both strains exhibit a rapid increase in Ras-GTP levels upon chemoattractant stimulation, which in wild-type cells peak at ~3–4 s after stimulation and then rapidly decrease to near-basal levels by ~10 s,

Table 1. Relative activity of Ras after cAMP stimulation using pulldown assays

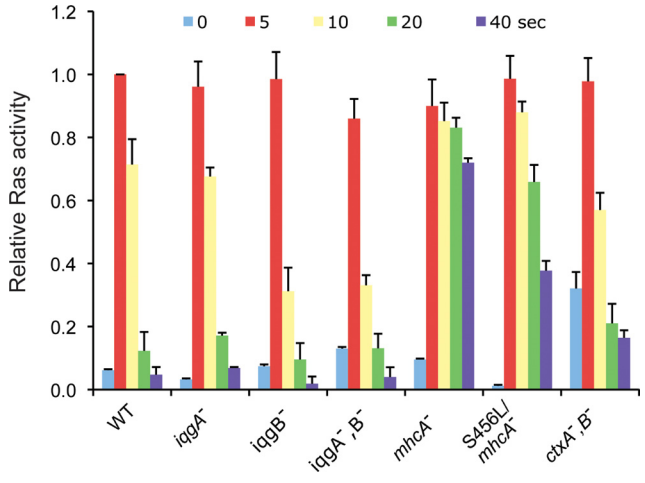

See Figure 1 and *Materials and Methods* for details.

as described previously (Sasaki *et al.*, 2004). In contrast, in *mhcA*$^-$ cells, the activity peaks later and exhibits a broader peak and a gradual decrease, consistent with the kinetics observed using the pulldown assay.

To determine if pathways downstream from Ras are extended in a similar manner, we used plasma membrane translocation of a GFP-PH domain reporter of PI(3,4,5)P_3 levels, GFP-PH_{PhdA}, to study the activation of the Ras-dependent effector PI3K (Parent *et al.*, 1998; Meili *et al.*, 1999; Funamoto *et al.*, 2002). Figure 1D illustrates that GFP-PH_{PhdA} plasma membrane localization rapidly increases, peaking at ~5–6 s after stimulation in wild-type and *mhcA*$^-$ cells and then rapidly decreasing to basal levels in wild-type cells, whereas in *mhcA*$^-$ cells, GFP-PH_{PhdA} remains at the plasma membrane for a considerably longer period of time. These findings suggest that the extended kinetics of Ras activation lead to extended PI3K activation. PI(3,4,5)P_3 levels are negatively regulated by the phosphatase PTEN, which is associated with the plasma membrane in unstimulated cells and then transiently delocalizes from the cortex (Funamoto *et al.*, 2002; Iijima and Devreotes, 2002). To distinguish between the extended PI3K activity being a function of extended Ras activity or changes in the kinetics of PTEN localization on the plasma membrane, we investigated the kinetics of cortical GFP-PTEN delocalization and rebinding in wild-type and *mhcA*$^-$ cells. We found the kinetics are indistinguishable, supporting the model in which extended PI3K activity is due to extended Ras activity (data not shown). However, we cannot distinguish between this model and one in which Ras-mediated PI3K activity is extended and PTEN enzyme activity is also decreased in *mhcA*$^-$ cells.

F-actin levels are regulated, in part, by the PI3K pathway (Iglesias and Devreotes, 2008; Janetopoulos and Firtel, 2008; Koelsch *et al.*, 2008; Kortholt and Van Haastert, 2008; King and Insall, 2009). To determine if the elevated and extended PI3K pathway results in a change in the F-actin profile, we examined the kinetics of F-actin polymerization in wild-type and *mhcA*$^-$ cells. As shown in Figure 1D, wild-type cells exhibit reciprocal, bimodal kinetics of chemoattractant-stimulated F-actin polymerization and MyoII polymerization, consistent with previous studies (Hall *et al.*, 1988; Moores *et al.*, 1996; Steimle *et al.*, 2001; Levi *et al.*, 2002). F-actin accumulation exhibits a first peak at ~5 s, after which F-actin levels decrease to near-basal levels with a trough at ~20 s, followed by a lower, broad second peak at ~30–45 s (Figure 1D; Hall *et al.*, 1988; Yumura and Fukui, 1998). In contrast, MyoII levels decrease slightly at 5 s, followed by a gradual rise, peaking at 20–40 s and then decreasing to basal levels as described previously (Bosgraaf *et al.*, 2002; Park *et al.*, 2004). We find that *mhcA*$^-$ cells exhibit a higher basal level of F-actin. On chemoattractant stimulation, the rapid increase in F-actin levels is similar in wild-type and *mhcA*$^-$ cells (first peak), but the second F-actin peak is much larger in *mhcA*$^-$ cells and starts to rise before the first peak has decreased much (Figure 1E). These findings suggest that the level of the second F-actin peak, which has been linked to pseudopod protrusion (Hall *et al.*, 1988), is modulated by assembled MyoII, consistent with a model in which MyoII must be disassembled at the site of F-actin polymerization for pseudopod extension.

Akt/PKB kinase activity depends on two Ras-mediated effector pathways: PI3K, which promotes the PIP3-dependent recruitment of Akt/PKB to the plasma membrane and regulates PDK1 phosphorylation of the Akt/PKB activation loop, and TORC2, which mediates Akt/PKB phosphorylation on the C-terminal hydrophobic motif (Meili *et al.*, 1999; Funamoto *et al.*, 2002; Lee *et al.*, 2005; Kamimura *et al.*, 2008). As depicted in Figure 2, A and B, and Table 2, Akt/PKB exhibits an elevated level and extended kinetics of Akt/PKB activation in *mhcA*$^-$ cells compared with those in wild-type cells, consistent with extended activation of Ras and PI3K. In addition, *Dictyostelium* has a second PKB-related enzyme that localizes to the plasma membrane constitutively through an N-terminal myristoylation, which makes PKBR1 activation PI3K-independent (Firtel and Meili, 2000). Like PKB, PKBR1 requires TORC2 to phosphorylate the C-terminal hydrophobic motif and to activate the enzyme. Figure 2, C and D, shows that, like Akt/PKB, PKBR1 activity is also highly elevated and extended, consistent with both TORC2 and PI3K being affected in *mhcA*$^-$ cells.

MyoII assembly/disassembly in *Dictyostelium* is regulated by the phosphorylation of three threonines ($Thr^{1823, 1833, 2029}$) in the coil-coiled domain by a family of four MyoII heavy-chain kinases (MHCK-A–D). Phosphorylation of these three sites causes MyoII filament disassembly, whereas dephosphorylation leads to MyoII assembly (Egelhoff *et al.*, 1993; Stites *et al.*, 1998; de la Roche *et al.*, 2002; Bosgraaf and Van Haastert, 2006). Substitutions of these threonine residues with alanines result in a MyoII that is constitutively assembled, whereas Asp substitutions produce a MyoII that does not assemble (Egelhoff *et al.*, 1993; de la Roche *et al.*, 2002). We found that Akt/PKB activation is suppressed in *mhcA*$^-$ cells expressing MyoII-3XAla, suggesting that constitutive MyoII assembly inhibits pathway activation (Figures 2, A and B; Table 2). In contrast, *mhcA*$^-$ cells expressing MyoII-3XAsp exhibit a pattern of extended activation similar to that observed in *mhcA*$^-$ cells and an activation peak that is between that of wild-type and *mhcA*$^-$cells. These findings are consistent with a model in which MyoII assembly dynamics are required for the rapid Ras/PI3K pathway adaptation. We examined this further by studying Akt/PKB activation in cells lacking MHCKs, which have elevated levels of assembled MyoII (Yumura *et al.*, 2005). Cells lacking MHCK-A exhibit activation kinetics that are slightly lower than those of wild-type cells (Table 2). However, disruption

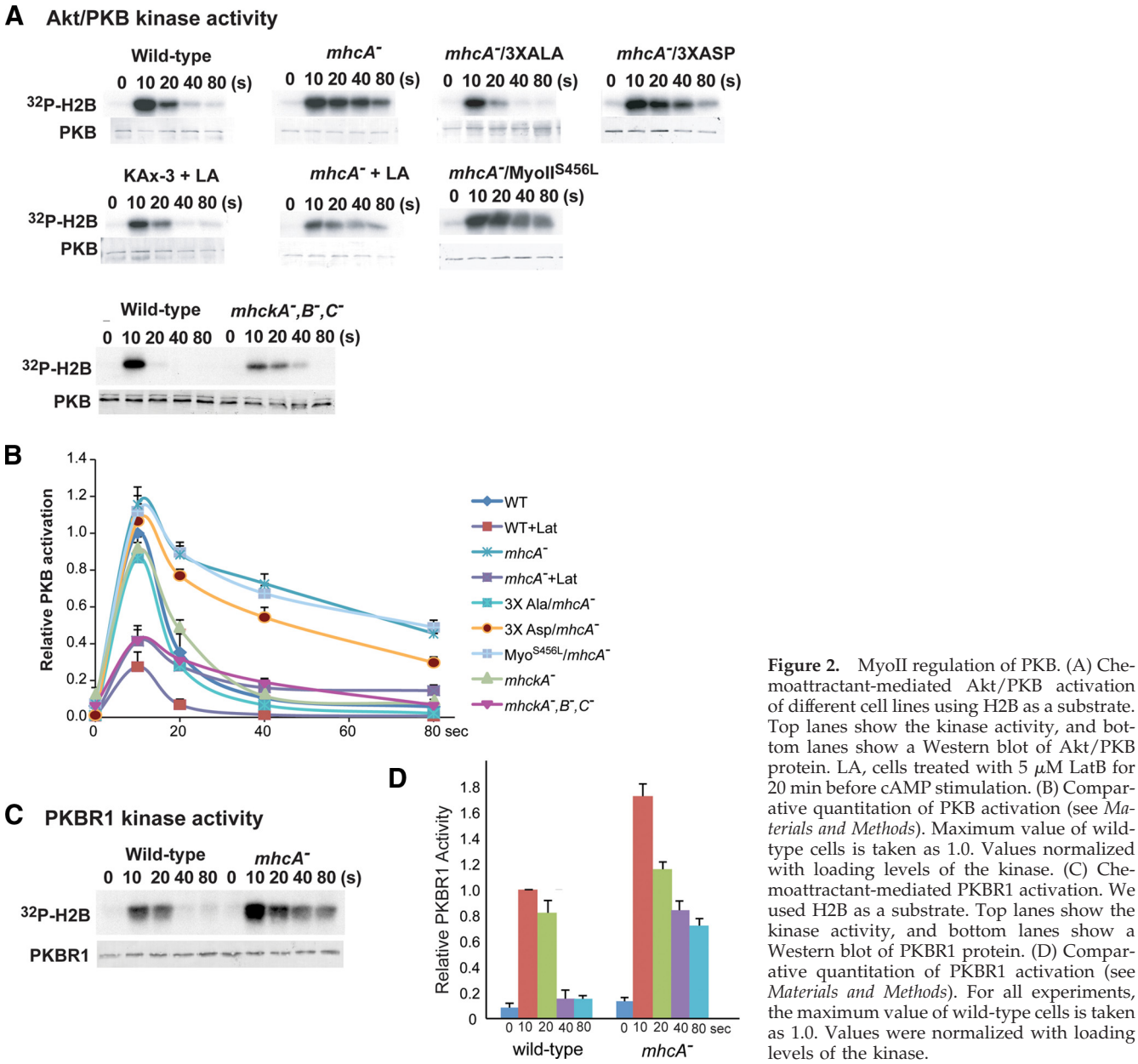

Figure 2. MyoII regulation of PKB. (A) Chemoattractant-mediated Akt/PKB activation of different cell lines using H2B as a substrate. Top lanes show the kinase activity, and bottom lanes show a Western blot of Akt/PKB protein. LA, cells treated with 5 μM LatB for 20 min before cAMP stimulation. (B) Comparative quantitation of PKB activation (see *Materials and Methods*). Maximum value of wild-type cells is taken as 1.0. Values normalized with loading levels of the kinase. (C) Chemoattractant-mediated PKBR1 activation. We used H2B as a substrate. Top lanes show the kinase activity, and bottom lanes show a Western blot of PKBR1 protein. (D) Comparative quantitation of PKBR1 activation (see *Materials and Methods*). For all experiments, the maximum value of wild-type cells is taken as 1.0. Values were normalized with loading levels of the kinase.

of MHCK-A, -B, and -C results in a considerable impairment of Akt/PKB activation, consistent with our model (Figure 2, A and B; Table 2).

We then investigated how MyoII activity might down-regulate Ras and PI3K activity by assaying Ras and Akt/PKB activation in *mhcA*$^-$ cells expressing MyoII^{S456A}, a MyoII mutant with impaired motor activity (Murphy *et al.*, 2001b; Reichl *et al.*, 2008; Ren *et al.*, 2009). We found that activation of Ras and PKB activity is extended in MyoII^{S456A}/*mhcA*$^-$ cells, although not to the extent observed in *mhcA*$^-$ cells, consistent with the reduced activity of this motor (Figures 1A and 2, A and B; Tables 1 and 2).

We demonstrated previously that F-actin polymerization is a component of a positive feedback loop that amplifies leading-edge responses and stabilizes a nascent leading edge, in part through the recruitment of PI3K (Sasaki *et al.*, 2004). Pretreatment of cells with latrunculin B (LatB), an F-actin inhibitor, dramatically reduces the level of chemoattractant-mediated PKB activation in both *mhcA*$^-$ and wild-type cells (Figure 2A; Table 1; Sasaki *et al.*, 2004), although PKB activity is still higher and more extended in *mhcA*$^-$ cells than in LatB-treated wild-type cells. These observations indicate that the extended PKB activation in *mhcA*$^-$ cells is not due to an enhanced positive feedback mediated by the elevated level of F-actin polymerization in these cells. Our findings are consistent with a model in which MyoII helps mediate the adaptation or restrict the activation of at least some early chemoattractant-mediated effector pathways.

MyoII Is Required for Proper Spatial Regulation of Ras and PI3K Pathways

To understand the effect of loss of MyoII on the spatial activation of Ras and PI3K pathways in vivo, we followed the spatiotemporal localization of GFP-RBD and GFP-

Table 2. Relative activity of Akt/PKB after cAMP stimulation using H2B as substrate

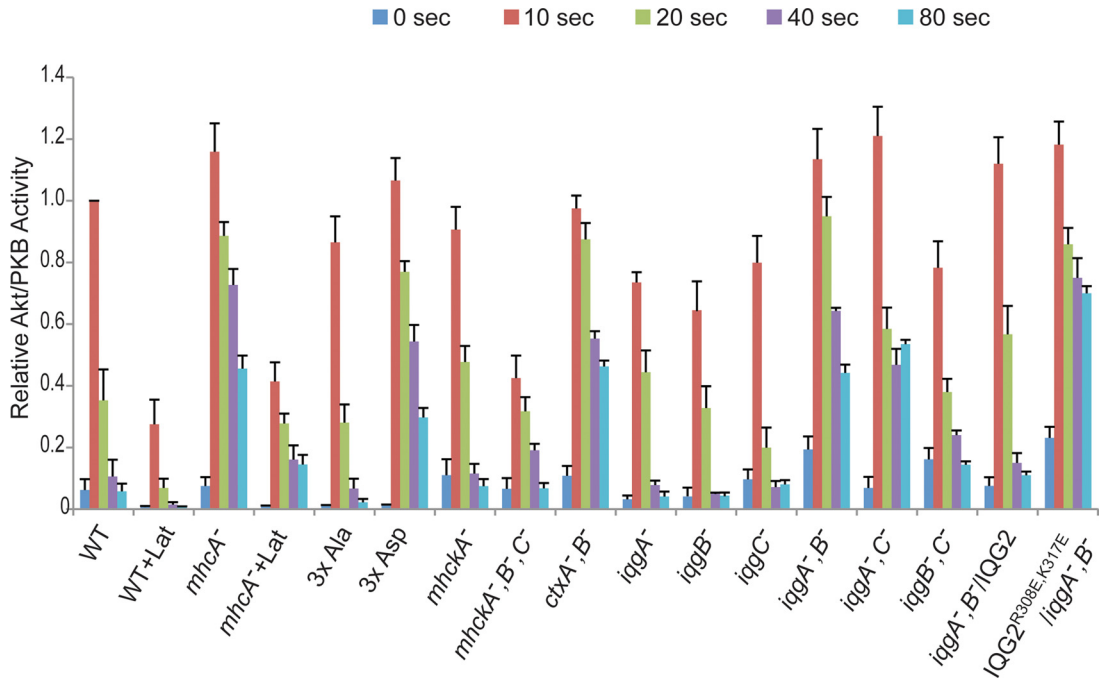

See Figure 2 and *Materials and Methods* for details. We quantified the $^{32}PO_4$ incorporation by using a Typhoon 9400 phosphorimager (GE Healthcare).

PH_{PhdA} in cells placed in a chemoattractant gradient. The localization of GFP-PH_{PhdA} and the Ras-GTP reporter GFP-RBD are correlated with the position of new F-actin polymerization and pseudopodial protrusions (Parent *et al.*, 1998; Meili *et al.*, 1999; Sasaki *et al.*, 2004). Whereas GFP-RBD and GFP-PH domain reporters localize almost exclusively to the site on the membrane closest to the chemoattractant source in wild-type cells, both reporters localize almost randomly in *mhcA*$^-$ cells (Figure 3). As *mhcA*$^-$cells respond to the chemoattractant gradient, activated Ras and $PI(3,4,5)P_3$ are often found in more than one domain on the cell cortex simultaneously. The domains of Ras and PI3K activity are generally much broader than those of wild-type cells, consistent with the inability of *mhcA*$^-$ cells to polarize efficiently.

To evaluate the role of elevated PI3K activity in mediating the increase in lateral pseudopod formation in *mhcA*$^-$cells, we examined the chemoattractant behavior of these cells treated with LY294002. As shown previously, LY294002 treatment considerably reduces chemoattractant speed and the extent of pseudopod extension in wild-type cells compared with untreated cells (quantitation of chemotaxis using DIAS software in Table 3; Supplemental Figures 1 and 2; Takeda *et al.*, 2007, Bosgraaf *et al.*, 2008). The LY294002-treated cells also undergo a moderate loss of directionality due to some pseudopodia localizing more randomly along the cell cortex. As described previously and reexamined here for comparison, *mhcA*$^-$ cells move more slowly and have a reduced directionality compared with wild-type cells because of a reduced ability to suppress lateral pseudopodia (Table 3; Supplemental Figure 2; Wessels *et al.*, 1988). Treatment of *mhcA*$^-$ cells with LY294002, as in wild-type cells, inhibits PI3K activity in these cells as determined by the abrogation of PH domain localization to the cell cortex in response to chemoattractant stimulation (data not shown). Analysis of LY294002-treated *mhcA*$^-$ cells chemotaxing cells shows that these cells have a further reduction of speed (Table 3) and the amount of pseudopod extension (Supplemental Figure 2) compared with *mhcA*$^-$ cells. Although the LY294002-treated *mhcA*$^-$ cells exhibit a modest increase in directionality, we note that they have a reduced ability to suppress lateral pseudopod formation compared with wild-type cells. The observations suggest that inhibition of PI3K reduces the extent of lateral pseudopod formation in *mhcA*$^-$ cells; however, these cells still exhibit a reduced polarity and directionality compared with LY294002-treated wild-type cells. We expect this reduction in polarity and directionality is due, in part, to the reduced and aberrant localization of traction forces observed in *mhcA*$^-$ cells due to loss of cortical tension and the ability to properly organize the cell cortex along the lateral sides and posterior of the cells (del Alamo *et al.*, 2007; Lombardi *et al.*, 2007; Meili *et al.*, 2010).

Composition of the IQGAP/ctx Complexes

The IQGAP/ctx complex is a key component of the cytoskeleton that also functions to cross-link F-actin and to mediate cortical tension (Ren *et al.*, 2009; Kee and Robinson, unpublished observations). Before examining the potential role of IQGAPs and ctxs in spatially and temporally controlling leading-edge pathways, we felt it was important to define the composition of the *Dictyostelium* IQGAP complexes. Previous studies demonstrated that DdIQGAP1 (DGAP1) interacts with ctxI and Rac1 in vegetative cells (Faix *et al.*, 1998; Weber *et al.*, 1999). (For simplicity and to conform to *Dictyostelium* gene nomenclature, we have renamed DGAP1, GAPA, and a third IQGAP we have identified as DdIQGAP1, DdIQGAP2, and

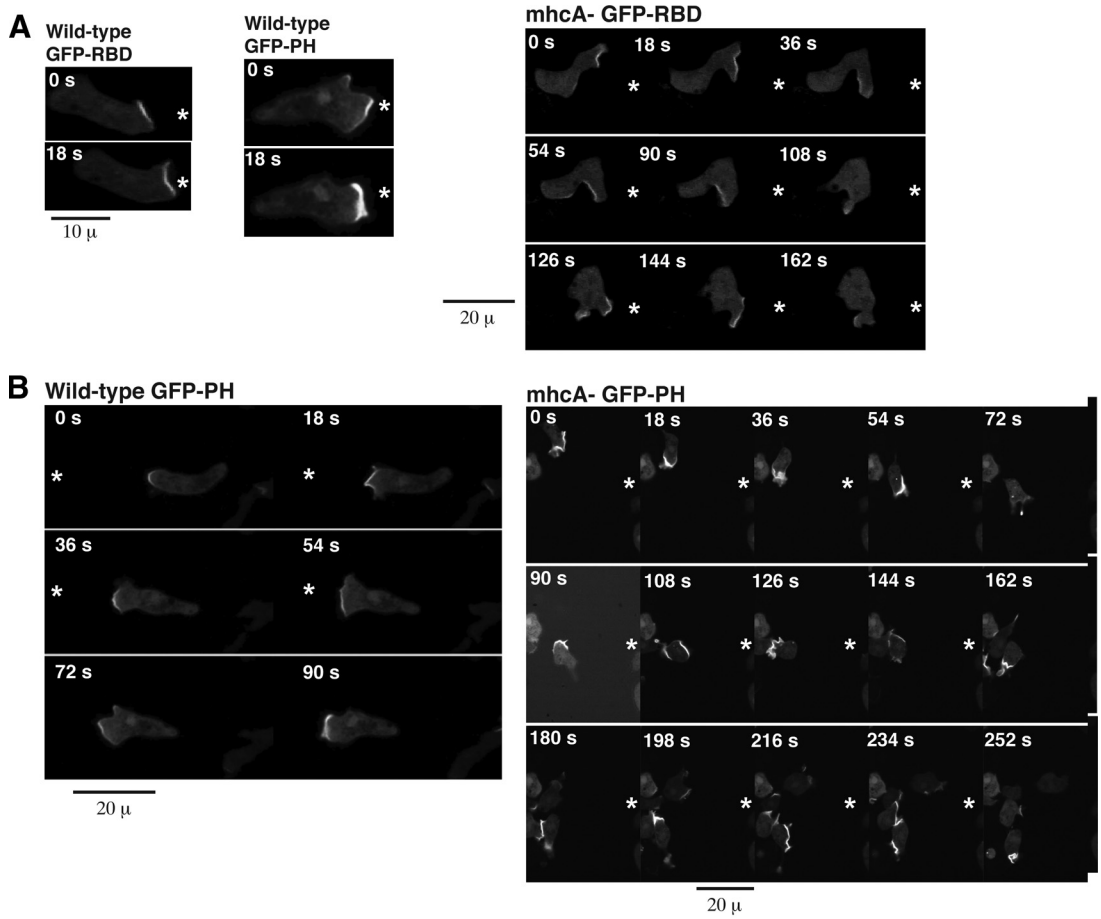

Figure 3. Spatial misregulation of Ras and PI3K activity in MyoII null cells. (A) A wild-type cell and an *mhcA*$^-$ cell expressing GFP-RBD were exposed to a chemoattractant gradient of cAMP emitted by a micropipette, and the localization of GFP-RBD was recorded. (B) A wild-type cell and *mhcA*$^-$ cells expressing GFP-PH were exposed to a chemoattractant gradient of cAMP emitted from a micropipette, and we recorded the localization of GFP-PH.

DdIQGAP3, respectively, and the respective genes as *iqgA, iqgB,* and *iqgC*.) To understand potential differences in function of DdIQGAP1 and DdIQGAP2 and to identify the components that interact with IQGAP1 and IQGAP2 during the aggregation stage of development when cells are competent to respond to cAMP as a chemoattractant, we used individually epitope-tagged DdIQGAP1 and DdIQGAP2 to purify complexes containing these proteins from vegetative cells and unstimulated and cAMP-stimulated developed (pulsed) cells. For both DdIQGAPs, we observed four major bands on silver-stained SDS-PAGE gels that were not found in the control samples (cells not expressing the epitope-tagged DdIQGAP; Figure 4), and the pattern of bands observed in samples from all of the cells were indistinguishable. Mass spectroscopy analysis revealed that the bands isolated using tagged DdIQGAP1 were DdIQGAP1, ctxI and ctxII, a previously undescribed cortexillin, ctxIII, and all three members of the Rac1 family: Rac1A, Rac1B, and Rac1C (Supplemental Figure 3). Using tagged DdIQGAP2 to isolate complexes, we identified DdIQGAP2, Rac1A, B, and C, and ctxI and II but not ctxIII (Figure 4). The low-mobility bands at ~200 kDa are most likely homodimers or a large multimeric complex of the IQGAP, because immunoblots of the gels revealed that the bands reacted with the epitope used to tag the IQGAP1 or IQGAP2, respectively. Complexes that contained both DdIQGAP1 and DdIQGAP2 were not observed. Two other proteins, HspE and rp17, were also found to be enriched in the complexes but were present at much lower stoichiometric levels than the other proteins and were not examined further (data not shown). Coimmunoprecipitation experiments using cells expressing the DdIQGAP1 or DdIQGAP2 tagged with one epitope and ctxIII with another epitope confirmed that DdIQGAP1, but not DdIQGAP2, coimmunoprecipated with ctxIII (Supplemental Figure 4).

IQGAPs Differentially Affect F-Actin Polymerization and MyoII Assembly and Cell Motility

To understand the potential roles each of these proteins play in chemotaxis, we undertook a more detailed examination of both *iqgA*$^-$ and *iqgB*$^-$ strains and created and studied *iqgC*$^-$, *iqgA*$^-$/*B*$^-$, *iqgA*$^-$/*C*$^-$, and *iqgB*$^-$/*C*$^-$ strains. Images of chemotaxing cells are presented in Figure 5 (some strains not shown), and the quantitation of chemotaxis using DIAS software is found in Table 3. When placed in a chemoattractant gradient, *iqgA*$^-$ cells have a speed slightly, but reproducibly, higher than wild-type cells and exhibit more lateral pseudopodia than wild-type cells. In contrast, *iqgB*$^-$ cells exhibit no change in speed but have a reduced directionality due to a reduced ability to suppress lateral pseudopodia,

Table 3. DIAS analysis of chemotaxis

	Strain background					
Parameters	Wild type	*iqgA*$^-$	*iqgB*$^-$	*iqgC*$^-$	*iqgA*$^-$/*B*$^-$	*iqgA*$^-$/*C*$^-$
Speed (μm/min)	10.5 ± 0.70	12.2 ± 0.84	10.3 ± 1.24	10.8 ± 1.00	4.03 ± 0.18	10.4 ± 0.54
Dir ch (deg)	24.3 ± 4.0	26.6 ± 3.32	67.4 ± 3.80	21.2 ± 2.27	71.7 ± 2.91	26.4 ± 2.95
Roundness	50.6 ± 3.0	60.7 ± 4.17	52.4 ± 1.70	44.6 ± 5.81	56.1 ± 10.6	74.9 ± 2.08
Directionality	0.76 ± 0.01	0.74 ± 0.03	0.64 ± 0.02	0.84 ± 0.02	0.25 ± 0.06	0.70 ± 0.07

	Strain background					
Parameters	*iqgB*$^-$/*C*$^-$	*ctxA*$^-$	*ctxB*$^-$	*ctxC*$^-$	*ctxA*$^-$/*B*$^-$	*mhcA*$^-$
Speed (μm/min)	4.99 ± 0.59	9.78 ± 2.43	11.4 ± 0.51	5.44 ± 0.91	9.19 ± 2.09	4.58 ± 1.43
Dir ch (deg)	44.5 ± 9.12	37.1 ± 1.75	24.3 ± 1.41	48.3 ± 11.4	33.6 ± 8.69	64.6 ± 17.5
Roundness	63.0 ± 5.32	49.1 ± 2.56	46.9 ± 4.99	55.5 ± 0.80	48.0 ± 4.68	79.7 ± 8.69
Directionality	0.64 ± 0.02	0.68 ± 0.02	0.73 ± 0.02	0.57 ± 0.11	0.62 ± 0.04	0.27 ± 0.22

	Vector					
Parameters	GAP1	GAP1 K273E, K282E	GAP1	GAP1 K273E, K282E	GAP1	K273E, K282E
Strain background	Wild type	Wild type	*iqgA*$^-$	*iqgA*$^-$	*iqggA*$^-$/*B*$^-$	*iqgA*$^-$/*B*$^-$
Speed (μm/min)	8.37 ± 1.11	7.94 ± 0.66	8.80 ± 0.77	5.54 ± 1.67	9.05 ± 3.91	6.59 ± 3.10
Dir ch (deg)	40.1 ± 5.12	48.1 ± 5.34	46.6 ± 6.81	68.6 ± 9.36	49.2 ± 20.7	56.5 ± 20.7
Roundness	58.3 ± 3.41	62.2 ± 5.91	49.9 ± 4.11	66.7 ± 9.55	74.4 ± 11.8	73.3 ± 13.9
Directionality	0.64 ± 0.02	0.55 ± 0.09	0.56 ± 0.06	0.29 ± 0.13	0.45 ± 0.25	0.34 ± 0.31

	Vector					
Parameters	GAP2	GAP2 R308E, K317E	GAP2	GAP2 R308E, K317E	GAP2	GAP2
Strain background	Wild type	Wild type	*iqgB*$^-$	*iqgB*$^-$	*iqgA*$^-$/*B*$^-$	*iqgA*$^-$/*B*$^-$
Seed (μm/min)	11.7 ± 2.92	11.1 ± 2.28	10.0 ± 0.79	7.60 ± 3.32	9.79 ± 4.45	4.51 ± 2.00
Dir ch (deg)	19.3 ± 11.9	22.9 ± 3.02	37.0 ± 11.2	46.7 ± 29.4	27.3 ± 13.3	69.1 ± 23.0
Roundness	66.7 ± 2.92	55.1 ± 0.82	53.0 ± 0.44	70.4 ± 14.7	79.3 ± 6.01	76.8 ± 8.30
Directionality	0.83 ± 0.11	0.78 ± 0.05	0.68 ± 0.08	0.51 ± 0.35	0.75 ± 0.10	0.20 ± 0.31

	Strain background	
Parameters	Wild type + LY	*mhcA*$^-$ + *LY*
Speed (μm/min)	4.01 ± 1.13	3.24 ± 0.88
Dir ch (deg)	38.9 ± 12.1	52.6 ± 14.4
Roundness	55.7 ± 0.39	82.6 ± 4.88
Directionality	0.61 ± 0.15	0.45 ± 0.29

Values are mean ± SD. Speed indicates the speed of cell's centroid movement along the total path. Direction change (Dir ch) is a relative measure of the number and frequency of turns the cell makes. Larger numbers indicate more turns and less efficient chemotaxis. Roundness is an indication of the polarity of the cells. Larger numbers indicate the cells are more round (less polarized). Directionality is a measure of the linearity of the pathway. Cells moving in a straight line to the chemoattractant-emitting micropipette have a directionality of 1.00.

similar to *mhcA*$^-$ cells (Table 3; Wessels *et al.*, 1988). *iqgC*$^-$ cells exhibit chemotaxis parameters similar to those of wild-type cells. Conversely, the *iqgA*$^-$/*B*$^-$ cells show very decreased speed, directionality, and cell polarity. These cells do not aggregate, consistent with their chemotaxis defects (data not shown). *iqgB*$^-$/*C*$^-$ cells also have a 50% reduction in speed, although the reduction in directionality is less than that for *iqgA*$^-$/*B*$^-$ cells. The *iqgA*$^-$/*C*$^-$ cells exhibit good directionality and speeds similar to those of wild-type cells, although they are less polarized than wild-type cells and have an increased orientation change. Our findings suggest that DdIQGAP2 is important for polarity and is required with DdIQGAP1 or DdIQGAP3 for functional chemotaxis. DdIQGAP1 and DdIQGAP3 may have overlapping genetic functions during chemotaxis and in controlling cell polarity.

To better understand the basis for the chemotaxis defects of the *IQGAP* null strains, we examined chemoattractant-mediated F-actin polymerization and MyoII assembly (Figure 6, A and B, respectively). The analysis indicates that, compared with wild-type cells, *iqgA*$^-$ cells exhibit a slight reduction in the first F-actin peak and a small increase in the second peak. In *iqgA*$^-$ cells, the peak of assembled MyoII is reduced considerably compared with that of wild-type cells. In contrast, *iqgB*$^-$ cells show a small increase in basal F-actin

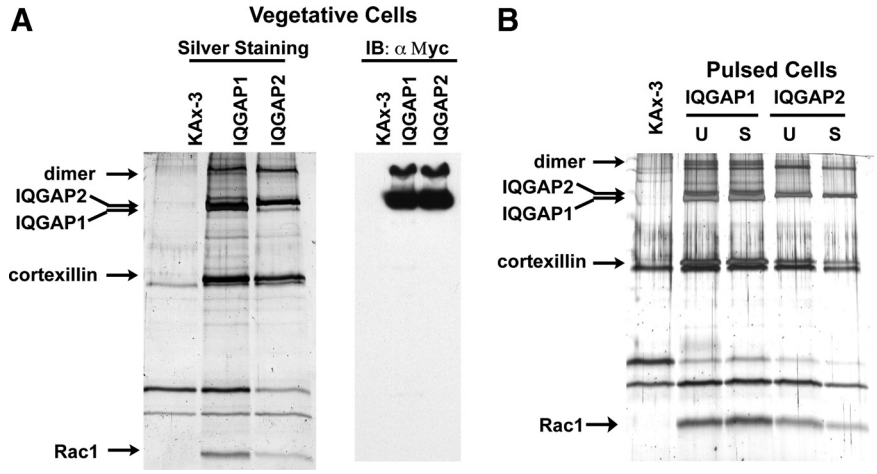

Figure 4. Isolation of IQGAP-containing complexes. (A) Silver staining of immunoprecipitated products with anti-Myc in vegetative KAx-3, Myc-IQGAP1/*iqgA*$^-$, and Myc-IQGAP2/*iqgB*$^-$ cells. Right panel depicts a Myc Western blot of the same samples. (B) Silver staining of pulsed KAx-3, Myc-IQGAP1/*iqgA*-, and IQGAP2/*iqgB*$^-$ cells unstimulated (U) and stimulated (S) cells.

levels, and a substantial increase in both F-actin peaks with a very small decline between the first and the second peak. Assembled MyoII is elevated in unstimulated *iqgB*$^-$ cells by ~30% and exhibits a much larger increase upon stimulation than that observed in wild-type cells. This chemoattractant-stimulated increase in assembled MyoII is elevated in *iqgB*$^-$ cells compared with that of wild-type cells even after normalization of the basal level of assembled MyoII.

iqgA$^-$/*B*$^-$ cells show a pattern similar to that of *iqgB*$^-$ cells, suggesting that the loss of DdIQGAP2 is the major determinant of the *iqgA*$^-$/*B*$^-$cell phenotype. *iqgC*$^-$ has an F-actin profile similar to that of wild-type cells. In *iqgA*$^-$/*C*$^-$ cells, the second F-actin peak is reduced compared with that in *iqgA*$^-$ cells, and *iqgB*$^-$/*C*$^-$ cells have an F-actin response that is higher than that of wild-type cells but lower than that of *iqgB*$^-$ cells. *iqgC*$^-$ and *iqgA*$^-$/*C*$^-$ have MyoII responses that are reduced compared with those of wild-type cells, whereas *iqgB*$^-$/*C*$^-$ cells exhibit a response similar to that of *iqgB*$^-$ cells. The analyses of the single and double knockout strains demonstrate that the loss of IQGAP2 results in a considerable increase in the F-actin response and an enhanced MyoII response. Loss of IQGAP1 causes a moderate increase in the responses, whereas the loss of IQGAP3 suppresses the responses. These data suggest that IQGAP2 behaves as a negative regulator and IQGAP3 is a positive modulator of the F-actin and MyoII responses.

As we showed previously, loss of both ctxI and ctxII, but not either protein alone, leads to an increased number of turns but only a small effect on directionality, and no effect on cell polarity or the speed of chemotaxis (Figure 5; Table 3; Jeon *et al.*, 2007). Loss of both proteins results in about a twofold increase in the second peak of F-actin polymerization and a modest reduction in the levels of chemoattractant-mediated MyoII assembly (Figure 5B). In contrast, loss of ctxIII causes a 50% reduction of speed and a decrease in directionality, but F-actin polymerization, MyoII assembly, and distribution of F-actin in phalloidin-stained cells are indistinguishable from those of wild-type cells. These findings suggest that ctxIII is an important regulator of chemotaxis but this regulation does not result from mediating the

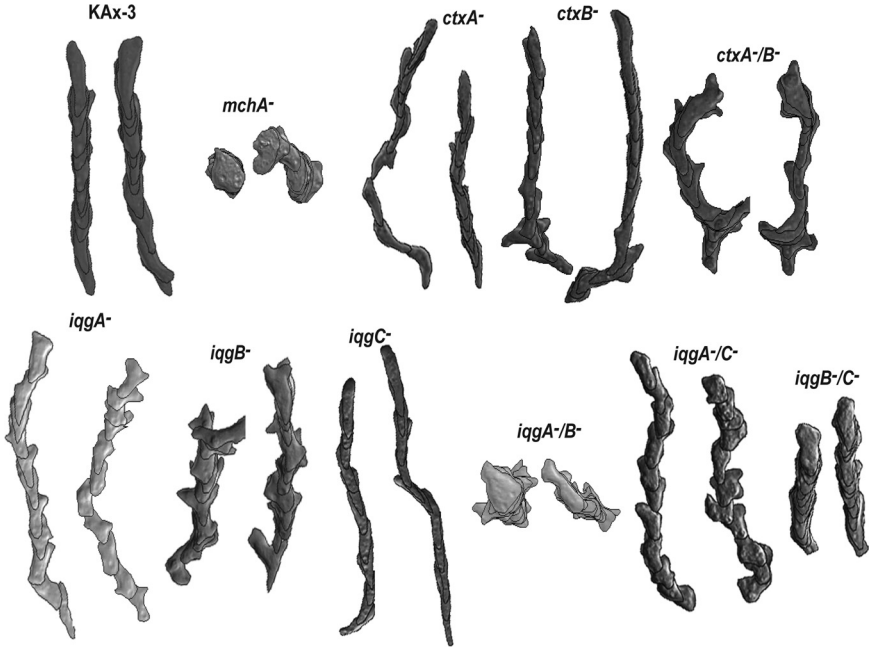

Figure 5. Images of chemotaxing cells obtained using DIAS computer software. The overlapping images were taken at 1-min intervals.

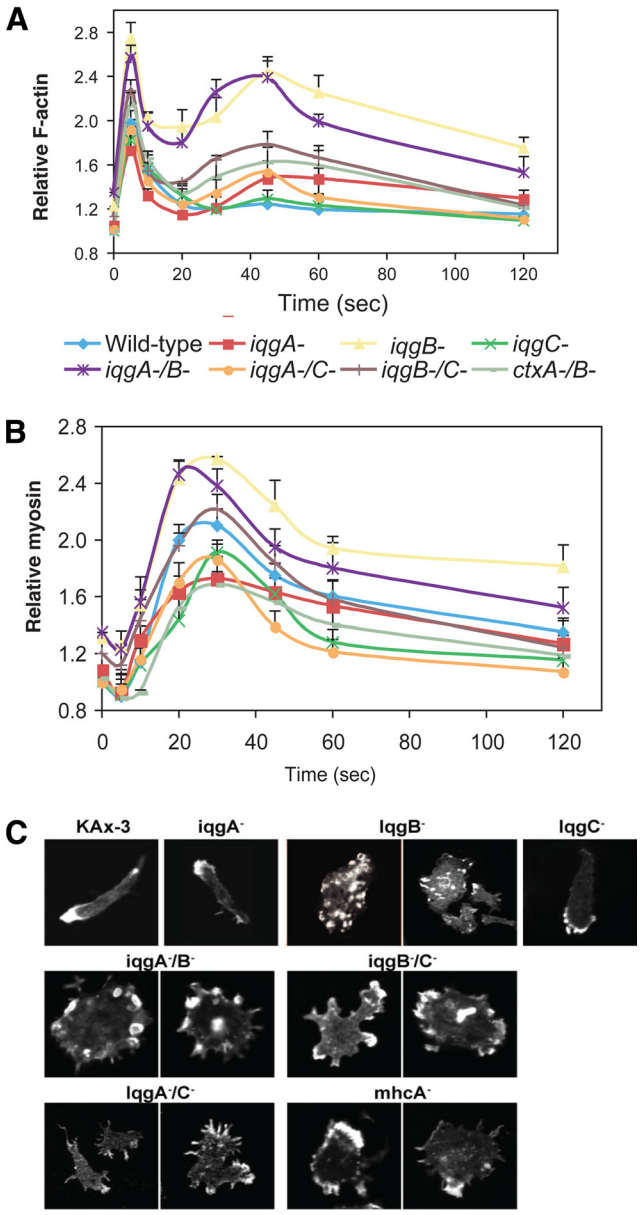

Figure 6. Kinetics of F-actin polymerization and MyoII assembly in IQGAP and ctx mutant strains. Kinetics of F-actin polymerization (A) and MyoII assembly (B) in the Triton-insoluble, cytoskeleton fraction. (C) Phalloidin staining of pulsed cells.

level or timing of the F-actin and MyoII responses (Figure 6, A and B; Table 3; data not shown).

To examine the spatial organization of F-actin in unstimulated, cAMP-responsive cells, we stained cells with FITC-phalloidin. Figure 6C illustrates that, like wild-type cells, *iqgC*$^-$ cells have a dominant F-actin–enriched pseudopod and a moderate level of filopodia (Figure 6C). *iqgA*$^-$ cells exhibit multiple thin, pseudopodia-like projects with F-actin localized at the ends of the projections. *iqgB*$^-$ cells have multiple, F-actin–enriched small projections, which may be filopodia. *iqgA*$^-$/*B*$^-$and *iqgB*$^-$/*C*$^-$ cells are round and have multiple, small F-actin–containing projections, some of which appear similar to be micropinosomes, structures that are not normally observed in developed cells. *iqgA*$^-$/*C*$^-$ cells have a combination of broad F-actin–containing, lamellipodia-like domains and enhanced, F-actin–containing filopodia-like spikes. These F-actin localization studies suggest that the three different IQGAPs play somewhat distinct roles in controlling the F-actin cytoskeleton.

IQGAPs, ctxI, and ctxII Are Required for PI3K and PKB But Not Ras Adaptation

Because of the abnormal patterns of F-actin polymerization and MyoII assembly, we studied the kinetics and level of Ras and PI3K activation in cells lacking different combinations of the three DdIQGAPs or ctx proteins. Figure 7, A and B, and Table 1 show that Ras activation is unaltered in two single *iqgap* null strains, a double mutant, and a double *ctx* null strain. When we examined PI3K activity indirectly by quantifying the level and kinetics of Akt/PKB activation, we found that the single *iqgap* and *ctx* null strains exhibited a normal level and kinetics of activation (Figure 7, C and D; Table 2; data not shown). However, cells lacking IQGAP2 in combination with either IQGAP1 or IQGAP3 (*iqgA*$^-$/*B*$^-$ and *igqA*$^-$/*C*$^-$ cells) exhibit highly elevated and extended PKB activation profiles. Cells lacking IQGAP2 and IQGAP3 (*igqA*$^-$/*C*$^-$ cells) have a slightly extended activation profile but with a lower level of PKB activation than wild-type cells. Cells lacking IQGAP2 in combination with IQGAP1 or IQGAP3 also exhibit the highest basal (unstimulated cells) levels of PKB activity. As shown in Figure 7, C and D, and Table 2, *ctxA*$^-$/*B*$^-$ cells display greatly extended kinetics of PKB activation but no increase in the peak level of activity.

To examine the possible basis for the extended activation of PKB in *igqA*$^-$/*B*$^-$ cells, we studied the kinetics of PI(3,4,5)P_3 levels by visualizing the subcellular localization of GFP-PH_{PhdA}. We found, as with *mhcA*$^-$ cells, *igqA*$^-$/*B*$^-$ cells exhibit a broad second peak that overlaps with the second peak of F-actin polymerization (Figure 8A). We then studied the kinetics of PI3K localization to the cell cortex in response to chemoattractant stimulation. As described previously (Funamoto *et al.*, 2002), in wild-type cells, PI3K is predominantly cytosolic and transiently localizes to the plasma membrane in response to chemoattractant stimulation with a peak at ~6 s followed by a slow delocalization from the cortex as shown either by time-lapse examination of GFP-PI3K fluorescence at the cell cortex or by examining the change in GFP-PI3K found in the Triton X-100–insoluble fraction, a method that provides a more quantitative analysis of PI3K protein levels in the cortex (Figure 8, B and D). In contrast, we find that *iqgA*$^-$/*B*$^-$ cells exhibit a highly elevated basal (unstimulated cells) level of PI3K at the cell cortex in both vegetative and aggregation-competent cells as indicated by level of GFP-PI3K fluorescence at the cell cortex and the amount of GFP-PI3K associated with the Triton X-100–insoluble fraction (Figure 8, C and D). On chemoattractant stimulation, *iqgA*$^-$/*B*$^-$ cells still exhibit an increase in cortically associated GFP-PI3K with a peak at ~6 s. However, the cortical level of PI3K only decreases slightly before increasing again with a second peak at 15–20 s, after which cortical levels decrease to basal levels. The timing of the second peak coincides with the second broad peak of PI(3,4,5)P_3 accumulation at the plasma membrane in these cells.

Rac1 Interaction Is Required for IQGAP Function

Rac1 and Cdc42 interact with mammalian IQGAPs. In *Dictyostelium*, which lacks Cdc42, only Rac1 has been found in the IQGAP-containing complexes that have been studied. An ~24-amino acid residue region (1054–1077) within the conserved RasGAP-related domain is required for Cdc42-

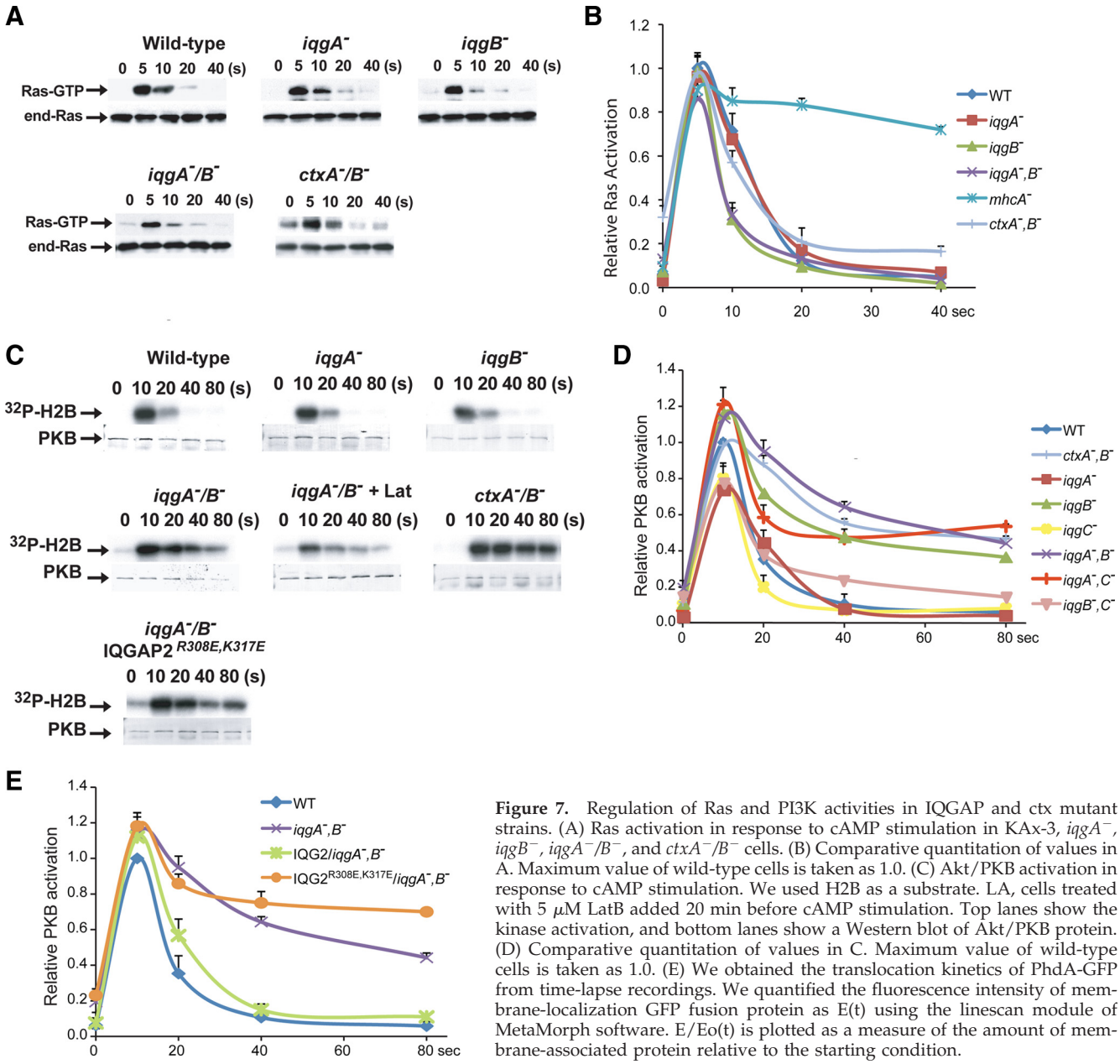

Figure 7. Regulation of Ras and PI3K activities in IQGAP and ctx mutant strains. (A) Ras activation in response to cAMP stimulation in KAx-3, *iqgA*$^-$, *iqgB*$^-$, *iqgA*$^-$/*B*$^-$, and *ctxA*$^-$/*B*$^-$ cells. (B) Comparative quantitation of values in A. Maximum value of wild-type cells is taken as 1.0. (C) Akt/PKB activation in response to cAMP stimulation. We used H2B as a substrate. LA, cells treated with 5 μM LatB added 20 min before cAMP stimulation. Top lanes show the kinase activation, and bottom lanes show a Western blot of Akt/PKB protein. (D) Comparative quantitation of values in C. Maximum value of wild-type cells is taken as 1.0. (E) We obtained the translocation kinetics of PhdA-GFP from time-lapse recordings. We quantified the fluorescence intensity of membrane-localization GFP fusion protein as E(t) using the linescan module of MetaMorph software. E/Eo(t) is plotted as a measure of the amount of membrane-associated protein relative to the starting condition.

GTP interaction with human IQGAP1 (Mataraza *et al.*, 2003). Sequence comparison determined that this region has a high degree of conservation between DdIQGAP1, DdIQGAP2, and human IQGAP1 (data not shown). To examine the role of Rac1-GTP interaction with IQGAP function in vivo, we created two point mutations in two conserved, charged residues, in each IQGAP in which the Lys or Arg residues are changed to Glu, IQGAP1$^{K273E,\ K282E}$ and IQGAP2$^{R308E,\ K317E}$, and found that the DdIQGAP1 carrying these mutations was no longer able to bind GST-Rac1A-GTP in a pulldown assay (Supplemental Figure 5). We then investigated the effect of Rac1 binding to the IQGAPs on PKB regulation. Expression of wild-type IQGAP2, but not the mutated IQGAP2$^{R308E,\ K317E}$, in *iqgA*$^-$/*iqgB*$^-$ cells does not complement the *iqgA*$^-$/*iqgB*$^-$ cell chemotaxis defects or the extended PKB activation (Tables 2 and 3; Figure 7E; data not shown), suggesting that Rac1-GTP interaction is required for IQGAP function.

DISCUSSION

Role of MyoII in Modulating Leading-Edge Pathways

The mechanisms that spatially and temporally restrict the signaling pathways regulating pseudopod formation are not well understood. Localized activation of RasG and RasC causes the localized activation of PI3K, TORC2, and other effectors that play major roles in forming a functional pseudopod (see *Introduction*). Positive feedback loops involving F-actin amplify the responses, stabilizing the leading edge, whereas negative regulators, including RasGAPs and PTEN, help restrict these pathways in space and time. The spatial distribution of PTEN and MyoII in an increasing anterior-to-posterior gradient suggests other regulatory events are important in restricting leading-edge pathways.

We examined the role of two different cytoskeletal complexes that help mediate cortical integrity by cross-linking

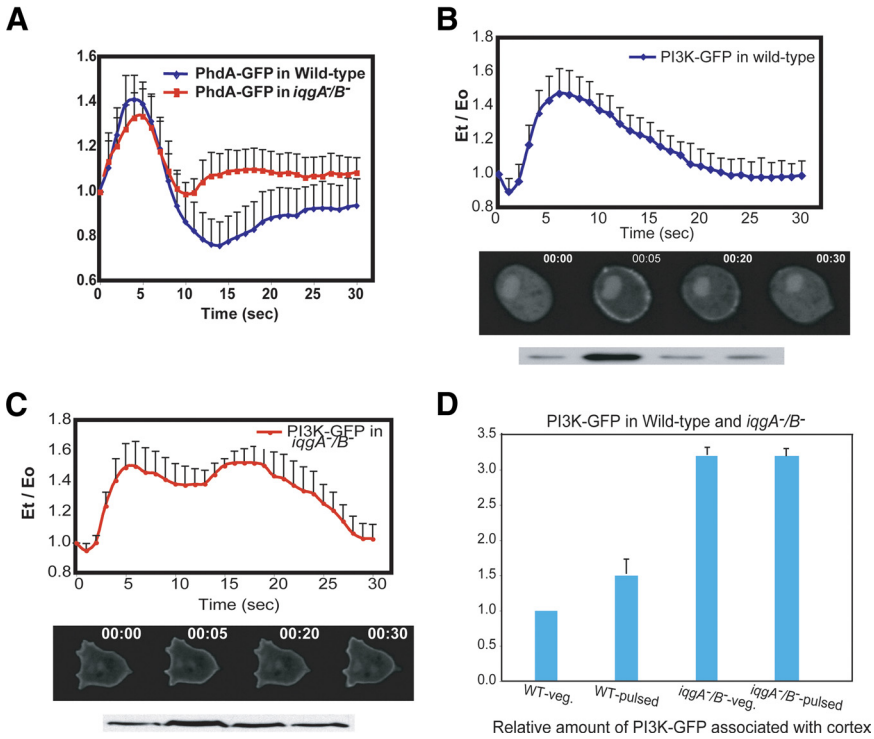

Figure 8. Kinetics of PI3K translocation to the cell cortex. (A) We obtained the translocation kinetics of PhdA-GFP from time-lapse recordings. We quantified the fluorescence intensity of membrane-localization GFP fusion protein as E(t) using the linescan module of MetaMorph software. E/Eo(t) is plotted as a measure of the amount of membrane-associated protein relative to the starting condition. (B and C) Chemoattractant-stimulated translocation of PI3K-GFP to the plasma membrane in wild-type (B) and *iqgA*$^{-}$/*B*$^{-}$ (C) cells. The middle panel shows the image from a time-lapse recording. The bottom panel shows the biochemical assay of PI3K-GFP. Cells were pushed through a Millipore membrane, and the membrane fractions were blotted with GFP antibody. (D) The basal level of PI3K-GFP in wild-type and *iqgA*$^{-}$/*B*$^{-}$ cells. The vegetative and pulsed cells were pushed through a Millipore membrane, and the membrane fractions were blotted with GFP and quantified.

F-actin in controlling leading-edge pathways known to promote F-actin polymerization and cell polarity. We demonstrate that MyoII plays a role in turning off chemoattractant-stimulated Ras activity and the absence of MyoII leads to extended activation of Ras-GTP levels, to the downstream increased and extended activation of PI3K and Akt/PKB, and to F-actin polymerization. We suggest that the defects in the *mhcA*$^{-}$ cells' Ras/PI3K and probably also Ras/TORC2 signaling pathways constitute an underlying factor in the previously described inability of these cells to inhibit lateral pseudopod formation (Wessels *et al.*, 1988). We attempted to examine the effect of deleting MyoII in RasC and RasG activation separately by expressing individually epitope-tagged versions of RasC and RasG in wild-type and *mhcA*$^{-}$ cells. Although we could overexpress tagged RasC in both strains, we could only overexpress RasG in wild-type cells. There was an insignificant extension of RasC activation, but as we were unable to overexpress RasG, we cannot determine if the effects observed are the result of extended activation of RasG and/or other Ras proteins.

Cells lacking MyoII exhibit an elevated basal level of Ras-GTP and a very extended activation profile. *mhcA*$^{-}$ cells expressing the MyoII uncoupler mutant MyoII^{S456L}, which has a 10-fold slower unloaded actin sliding velocity due to a one-quarter productive working stroke and threefold slower ADP release rate (under no-load conditions; Murphy *et al.*, 2001a), also exhibit extended Ras activity but not to the level of *mhcA*$^{-}$ cells. In our previous studies of S456L MyoII, we found that mechanical stress can partially rescue this motor. Therefore, the cell cortex of developed chemotaxing cells is likely to be weakly mechanically stressed, allowing this motor to provide partial function in restricting Ras and PI3K activity (Girard *et al.*, 2006; Reichl *et al.*, 2008, Ren *et al.*, 2009). As described previously, *myoII* null cells cannot restrict lateral pseudopod formation (Wessels *et al.*, 1988). Our findings suggest that the lateral pseudopodia occur at sites of Ras/PI3K activation that would normally be inhibited from occurring in wild-type cells. In *mhcA*$^{-}$ cells, areas of the cortex lacking MyoII are permissive for Ras/PI3K activation, suggesting why in highly polarized cells a very localized MyoII cortex is less responsive to the formation of new pseudopodia along the lateral sides than less polarized cells, even though receptors/G$\alpha\beta\gamma$ are present and become activated. As there is unregulated and extended activation of RasG and PI3K (e.g., *nfA*$^{-}$ and *pten*$^{-}$ cells, respectively; Funamoto *et al.*, 2002; Iijima and Devreotes, 2002), we suggest that these lateral pseudopodia result from an inability to restrict Ras activity, leading to activation of a PI3K/F-actin pathway. Once activated, the previously described positive feedback loops involving F-actin in which PI3K and RacGEFs are recruited to these sites would amplify the response and cause the robust formation of a new pseudopod. We suggest that in wild-type cells, as a leading edge forms and the cell polarizes, MyoII is disassembled at this site through the activation of Rap1 and the recruitment of MHCKs (Jeon *et al.*, 2007), whereas MyoII assembly and cortical localization are promoted along the lateral sides and posterior of the cell. Our findings suggest that one role for MyoII is to inhibit at least some leading-edge functions, which would help restrict leading-edge functions to the leading edge, whereas F-actin assembly at the new leading edge is involved in a positive feedback loop with PI3K (Sasaki *et al.*, 2004, 2007; Charest and Firtel, 2006). We suggest that this combination of positive and negative feedback loops between leading edge and lateral/posterior pathways is part of the mechanism that enhances cell polarity. As the cell starts to polarize in response to a directional chemoattractant signal, the localization of MyoII to the posterior helps restrict the response to the leading edge by blocking Ras activation. Whether this "inhibition" afforded by MyoII takes place by physically blocking access to the receptor/Gα/G$\beta\gamma$ (which are activated in proportion to the concentration of the chemoattractant) or through another mechanism is not known. Inhibition of PI3K with LY294002 suppresses cell speed and

pseudopod extension in *mhcA*$^-$ cells as it does for wild-type cells, which is consistent with this model (this article; Takeda *et al.*, 2007, Bosgraaf *et al.*, 2008). However, loss of MyoII also results in major changes in the level and organization of traction forces, presumably the result of loss of both F-actin cross-linking and motor function that plays a major role in the inability of *mhcA*$^-$ cells to suppress lateral pseudopodia (del Alamo *et al.*, 2007; Lombardi *et al.*, 2007; Meili *et al.*, 2010).

Roles of IQGAPs and ctxs in Regulating Ras and PI3K

We found that IQGAPs and ctxs, which bind and cross-link F-actin, also play an important role in controlling F-actin polymerization and MyoII assembly, and they are important in controlling the kinetics of the PI3K pathway. In agreement with previous studies, we observed that both IQGAP1 and IQGAP2 bind to one or more ctx proteins and Rac1. The association of ctx presumably provides the F-actin–binding activity found in the mammalian IQGAPs. We observe, however, that different ctx proteins interact with the different IQGAPs, which may indicate that individual IQGAP/ctx complexes have different functions. We determined that the individual mutant strains have different chemotaxis phenotypes, suggesting that they are not fully redundant. Mutating two conserved residues in the IQGAP1 RasGAP-related Rac1-GTP in the binding domain abrogates Rac1-GTP binding and the inability of the protein to complement the severe phenotypes of *iqgA*$^-$*/B*$^-$ cells. This finding suggests that Rac-GTP binding is required for IQGAP function, consistent with models for the involvement of Rac1/Cdc42-GTP binding in mammalian IQGAP function.

We characterized the chemotaxis phenotypes of IGAPA, B, and C and ctxI, II, and III and different double knockout combinations. *iqgB*$^-$ cells exhibit moderate chemotaxis defects as suggested previously: the cells are less polarized than wild-type cells and have a partial loss of lateral pseudopod inhibition. The phenotype of *iqgA*$^-$ cells is mild and *iqgC*$^-$ cells are even more polarized than wild-type cells and move slightly faster. *iqgA*$^-$*/B*$^-$ cells exhibit severe polarity and motility defects, whereas *iqgA*$^-$*/C*$^-$ cells have mild defects, although both strains exhibit multiple F-actin protrusions along the cortex of pulsed cells. Both *iqgB*$^-$ and *iqgA*$^-$*/B*$^-$ display similar levels of increased basal and chemoattractant-stimulated F-actin and assembled MyoII, even though only the double knockout shows the severe chemotaxis phenotype.

In conclusion, we have identified key roles for components of the cortical system in controlling the levels and extent of leading-edge pathways. MyoII is required for restricting the activation of Ras along the lateral sides and back of the cell and, we suggest, suppresses the formation of lateral pseudopodia by inhibiting one of the earliest steps in the pathway. We cannot, however, exclude the possibility that loss of MyoII may also directly affect PI3K activation independent of an effect on Ras. The IQGAP/ctx/Rac1 complex plays a different role and modulates F-actin and MyoII.

A Model by Which MyoII, ctx, and IQGAPs May Regulate Chemotaxis Signaling

The data presented here demonstrate that MyoII and ctx impact the signaling pathways of chemotaxis and provide evidence that they inhibit "front-end" signaling. Mechanistically, how might this cross-talk occur? First and foremost, the actin cytoskeletal network of a *Dictyostelium* cell is largely elastic with a mechanical phase angle of ~15° (where 0° is a solid and 90° is a liquid), implying that the cortex is largely solid-like (elastic; Girard *et al.*, 2004; Reichl *et al.*, 2008). Because signals can propagate through an elastic network over long distances and on much faster time scales than can occur by diffusion alone (Wang and Suo, 2005), an attractive idea is that this signal propagation occurs directly through the elastic network, which has properties defined in part by MyoII and ctx (Girard *et al.*, 2004; Reichl *et al.*, 2008). Both MyoII and ctx contribute ~20–30% to cortical viscoelasticity and to cortical tension. Particularly in dividing cells, mechanical stresses in the elastic network can also direct the accumulation of MyoII and ctxI, which work cooperatively to sense and accumulate locally in response to applied mechanical stress (Ren *et al.*, 2009). Interestingly, IQGAP2, but not IQGAP1, is required for mechanosensitive localization of ctx and MyoII (Kee and Robinson, unpublished data). Thus, the IQGAP proteins clearly define different populations of ctx with different mechanosensitive properties. IQGAP1 may define a ctx complex that is more dependent on chemical signal transduction, whereas IQGAP2 defines a ctx pool that is more responsive to mechanical stress inputs. By then coupling distinct signaling elements to the different IQGAPs, these downstream signaling cascades would become part of a mechano-chemical signal transduction system. As IQGAP2 plays a greater role in chemotactic signaling, it is possible that at least part of this signal relay between the two ends of the polarized cell occurs from mechanical stresses propagated directly through the elastic cytoskeleton.

Internally generated mechanical stresses may help drive accumulation of MyoII and ctx at the rear of a chemotaxing cell. The cell may initiate chemotaxis signaling using chemical inputs that trigger new F-actin assembly at the front of the cell. As these newly nucleated filaments push on the front of the cell, mechanical stresses are then sensed by the MyoII-ctx-IQGAP2 system. Of course, this MyoII-ctx-IQGAP2 system would not accumulate at the front of the cell because of the local activation of myosin heavy-chain kinases. However, the mechanosensitive accumulation of these complexes along the lateral and rear cortex would serve as a positive feedback on the signal, and, because they also stiffen the network, these proteins would suppress pseudopodial protrusion along these cortical domains. Consistently, softening of the elastic cortex twofold by depletion of another cross-linker (dynacortin), which enriches at the front and in pseudopodia, leads to a loss of cell polarity and more pseudopodia extending over a broader distribution of angles (Kabacoff *et al.*, 2007; Reichl *et al.*, 2008). The MyoII-ctx-IQGAP2 system may then convey an inhibitory signal on PI3K, perhaps by providing a positive feedback on PTEN accumulation in the cortex (Pramanik *et al.*, 2009).

Another aspect of how MyoII contributes to cortical dynamics is by modulating the active (superdiffusive) nature of the cortex (Girard *et al.*, 2006). These superdiffusive properties were originally detected by tracking the fluctuations of surface-attached particles, which then report on the underlying cortical dynamics. *mhcA*$^-$ cell cortices are considerably depleted of these superdiffusive activities; however, depletion of dynacortin in a *myoII* null cell substantially restores them. Observations such as this suggest that MyoII antagonizes some F-actin–associated proteins, perhaps by "kicking" or "stirring" the actin filaments, which may loosen the F-actin cross-linkers and/or associated proteins (this feature is in contrast to the cooperative interactions between MyoII and ctx). Thus, MyoII potentiates, rather than drives, the superdiffusive activities much like traffic signals potentiate the flow of traffic through a city. This antagonistic relationship between MyoII and some actin-associated proteins such as dynacortin may help explain the enhanced actin assembly in

the *mhcA*$^-$ cells. Through a process of elimination, although not directly proven, microtubules are proposed to be the source of the superdiffusive activities (Girard *et al.*, 2006). Microtubules might make contact with the cortex and help modulate the chemotactic signaling. At least one protein, tsunami, is associated with the microtubule network and contributes to cell polarization during chemotaxis (Tang *et al.*, 2008). Furthermore, if signaling complexes are coupled to F-actin–associated proteins that interact antagonistically with MyoII, then MyoII enrichment in part of the cell would help to shut off those signals. Clearly, Ras appears to be directly or indirectly inhibited through MyoII-mediated mechanochemical signal transduction, suggesting such a mechanism. In summary, the integration of mechanical with signaling observations suggests several novel hypotheses for how signal propagation through the cell may coordinate front and rear modules that reinforce cell polarity to drive efficient chemotaxis.

ACKNOWLEDGMENTS

We thank Pascale Charest and Alessia Para for critically reading the manuscript and all members of the Firtel laboratory for helpful suggestions. This work was supported by the following grants: National Institutes of Health (NIH) R01 GM037830 to R.A.F. and NIH Grant GM066817 and American Cancer Society Grant RSG CCG-114122 to D.N.R.

REFERENCES

Adachi, H., Takahashi, Y., Hasebe, T., Shirouzu, M., Yokoyama, S., and Sutoh, K. (1997). *Dictyostelium* IQGAP-related protein specifically involved in the completion of cytokinesis. J. Cell Biol. *137*, 891–898.

Bensenor, L. B., Kan, H. M., Wang, N., Wallrabe, H., Davidson, L. A., Cai, Y., Schafer, D. A., and Bloom, G. S. (2007). IQGAP1 regulates cell motility by linking growth factor signaling to actin assembly. J. Cell Sci. *120*, 658–669.

Bolourani, P., Spiegelman, G. B., and Weeks, G. (2006). Delineation of the roles played by RasG and RasC in cAMP-dependent signal transduction during the early development of *Dictyostelium discoideum.* Mol. Biol. Cell *17*, 4543–4550.

Bosgraaf, L., Russcher, H., Smith, J. L., Wessels, D., Soll, D. R., and Van Haastert, P. J. (2002). A novel cGMP signalling pathway mediating myosin phosphorylation and chemotaxis in *Dictyostelium.* EMBO J. *21*, 4560–4570.

Bosgraaf, L., and Van Haastert, P. J. (2006). The regulation of myosin II in *Dictyostelium.* Eur. J. Cell Biol. *85*, 969–979.

Bosgraaf, L., Keizer-Gunnink, I., and Van Haastert, P. J. (2008). PI3-kinase signaling contributes to orientation in shallow gradients and enhances speed in steep chemoattractant gradients. J. Cell Sci. *121*, 3589–3597.

Brandman, O., and Meyer, T. (2008). Feedback loops shape cellular signals in space and time. Science *322*, 390–395.

Brandt, D. T., and Grosse, R. (2007). Get to grips: steering local actin dynamics with IQGAPs. EMBO Rep. *8*, 1019–1023.

Briggs, M. W., and Sacks, D. B. (2003). IQGAP proteins are integral components of cytoskeletal regulation. EMBO Rep. *4*, 571–574.

Charest, P. G., and Firtel, R. A. (2006). Feedback signaling controls leading-edge formation during chemotaxis. Curr. Opin. Genet. Dev. *16*, 339–347.

Chen, L., Janetopoulos, C., Huang, Y. E., Iijima, M., Borleis, J., and Devreotes, P. N. (2003). Two phases of actin polymerization display different dependencies on PI(3,4,5)P_3 accumulation and have unique roles during chemotaxis. Mol. Biol. Cell *14*, 5028–5037.

Chung, C. Y., Lee, S., Briscoe, C., Ellsworth, C., and Firtel, R. A. (2000). Role of Rac in controlling the actin cytoskeleton and chemotaxis in motile cells. Proc. Natl. Acad. Sci. USA *97*, 5225–5230.

de la Roche, M. A., and Cote, G. P. (2001). Regulation of *Dictyostelium* myosin I and II. Biochim. Biophys. Acta *1525*, 245–261.

de la Roche, M. A., Smith, J. L., Betapudi, V., Egelhoff, T. T., and Cote, G. P. (2002). Signaling pathways regulating *Dictyostelium* myosin II. J. Muscle Res. Cell Motil. *23*, 703–718.

del Alamo, J. C., Meili, R., Alonso-Latorre, B., Rodriguez-Rodriguez, J., Aliseda, A., Firtel, R. A., and Lasheras, J. C. (2007). Spatio-temporal analysis of eukaryotic cell motility by improved force cytometry. Proc. Natl. Acad. Sci. USA *104*, 13343–13348.

Egelhoff, T. T., Lee, R. J., and Spudich, J. A. (1993). *Dictyostelium* myosin heavy chain phosphorylation sites regulate myosin filament assembly and localization in vivo. Cell *75*, 363–371.

Egelhoff, T. T., Naismith, T. V., and Brozovich, F. V. (1996). Myosin-based cortical tension in *Dictyostelium* resolved into heavy and light chain-regulated components. J. Muscle Res. Cell Motil. *17*, 269–274.

Eng, K., Naqvi, N. I., Wong, K. C., and Balasubramanian, M. K. (1998). Rng2p, a protein required for cytokinesis in fission yeast, is a component of the actomyosin ring and the spindle pole body. Curr. Biol. *8*, 611–621.

Faix, J., Clougherty, C., Konzok, A., Mintert, U., Murphy, J., Albrecht, R., Muhlbauer, B., and Kuhlmann, J. (1998). The IQGAP-related protein DGAP1 interacts with Rac and is involved in the modulation of the F-actin cytoskeleton and control of cell motility. J. Cell Sci. *111*, 3059–3071.

Faix, J., Weber, I., Mintert, U., Kohler, J., Lottspeich, F., and Marriott, G. (2001). Recruitment of cortexillin into the cleavage furrow is controlled by Rac1 and IQGAP-related proteins. EMBO J. *20*, 3705–3715.

Firtel, R. A., and Meili, R. (2000). *Dictyostelium*: a model for regulated cell movement during morphogenesis. Curr. Opin. Genet. Dev. *10*, 421–427.

Funamoto, S., Meili, R., Lee, S., Parry, L., and Firtel, R. A. (2002). Spatial and temporal regulation of 3-phosphoinositides by PI 3-kinase and PTEN mediates chemotaxis. Cell *109*, 611–623.

Funamoto, S., Milan, K., Meili, R., and Firtel, R. A. (2001). Role of phosphatidylinositol 3′ kinase and a downstream pleckstrin homology domain-containing protein in controlling chemotaxis in *Dictyostelium.* J. Cell Biol. *153*, 795–810.

Gebbie, L., *et al.* (2004). Phg2, a kinase involved in adhesion and focal site modeling in *Dictyostelium.* Mol. Biol. Cell *15*, 3915–3925.

Girard, K., Chaney, C., Delannoy, M., Kuo, S., and Robinson, D. (2004). Dynacortin contributes to cortical viscoelasticity and helps define the shape changes of cytokinesis. EMBO J. *23*, 1536–1546.

Girard, K., Kuo, S., and Robinson, D. (2006). *Dictyostelium* myosin-II mechanochemistry promotes active behavior of the cortex on long time-scales. Proc. Natl. Acad. Sci. USA *103*, 2103–2108.

Hall, A. L., Schlein, A., and Condeelis, J. (1988). Relationship of pseudopod extension to chemotactic hormone-induced actin polymerization in amoeboid cells. J. Cell. Biochem. *37*, 285–299.

Iglesias, P. A., and Devreotes, P. N. (2008). Navigating through models of chemotaxis. Curr. Opin. Cell Biol. *20*, 35–40.

Iijima, M., and Devreotes, P. (2002). Tumor suppressor PTEN mediates sensing of chemoattractant gradients. Cell *109*, 599–610.

Insall, R. H., Soede, R. D., Schaap, P., and Devreotes, P. N. (1994). Two cAMP receptors activate common signaling pathways in *Dictyostelium.* Mol. Biol. Cell *5*, 703–711.

Janetopoulos, C., and Firtel, R. A. (2008). Directional sensing during chemotaxis. FEBS Lett. *582*, 2075–2085.

Jeon, T. J., Lee, D. J., Merlot, S., Weeks, G., and Firtel, R. A. (2007). Rap1 controls cell adhesion and cell motility through the regulation of myosin II. J. Cell Biol. *176*, 1021–1033.

Jin, T., Xu, X., and Hereld, D. (2008). Chemotaxis, chemokine receptors and human disease. Cytokine *44*, 1–8.

Kabacoff, C., Xiong, Y., Musib, R., Reichl, E. M., Kim, J., Iglesias, P. A., and Robinson, D.N. (2007). Dynacortin facilitates polarization of chemotaxing cells. BMC Biol. *5*, *53.*

Kae, H., Kortholt, A., Rehmann, H., Insall, R. H., Van Haastert, P. J., Spiegelman, G. B., and Weeks, G. (2007). Cyclic AMP signalling in *Dictyostelium*: G-proteins activate separate Ras pathways using specific RasGEFs. EMBO Rep. *8*, 477–482.

Kamimura, Y., Xiong, Y., Iglesias, P. A., Hoeller, O., Bolourani, P., and Devreotes, P. N. (2008). PIP3-independent activation of TorC2 and PKB at the cell's leading edge mediates chemotaxis. Curr. Biol. *18*, 1034–1043.

Kehrl, J. H. (2006). Chemoattractant receptor signaling and the control of lymphocyte migration. Immunol. Res. *34*, 211–227.

King, J. S., and Insall, R. H. (2009). Chemotaxis: finding the way forward with *Dictyostelium.* Trends Cell Biol. *19*, 523–530.

Koelsch, V., Charest, P. G., and Firtel, R. A. (2008). The regulation of cell motility and chemotaxis by phospholipid signaling. J. Cell Sci. *121*, 551–559.

Kortholt, A., Rehmann, H., Kae, H., Bosgraaf, L., Keizer-Gunnink, I., Weeks, G., Wittinghofer, A., and Van Haastert, P. J. (2006). Characterization of the GbpD-activated Rap1 pathway regulating adhesion and cell polarity in *Dictyostelium discoideum.* J. Biol. Chem. *281*, 23367–23376.

Kortholt, A., and Van Haastert, P. J. (2008). Highlighting the role of Ras and Rap during *Dictyostelium* chemotaxis. Cell Signal. *20*, 1415–1422.

Laevsky, G., and Knecht, D. A. (2003). Cross-linking of actin filaments by myosin II is a major contributor to cortical integrity and cell motility in restrictive environments. J. Cell Sci. *116*, 3761–3770.

Lee, S., Comer, F. I., Sasaki, A., McLeod, I. X., Duong, Y., Okumura, K., Yates, J. R., 3rd, Parent, C. A., and Firtel, R. A. (2005). TOR complex 2 integrates cell movement during chemotaxis and signal relay in *Dictyostelium.* Mol. Biol. Cell *16*, 4572–4583.

Lee, S., Escalante, R., and Firtel, R. A. (1997). A Ras GAP is essential for cytokinesis and spatial patterning in *Dictyostelium.* Development *124*, 983–996.

Lee, S., Parent, C. A., Insall, R., and Firtel, R. A. (1999). A novel Ras-interacting protein required for chemotaxis and cyclic adenosine monophosphate signal relay in *Dictyostelium.* Mol. Biol. Cell *10*, 2829–2845.

Levi, S., Polyakov, M. V., and Egelhoff, T. T. (2002). Myosin II dynamics in *Dictyostelium*: determinants for filament assembly and translocation to the cell cortex during chemoattractant responses. Cell Motil. Cytoskelet. *53*, 177–188.

Li, Z., Dong, X., Wang, Z., Liu, W., Deng, N., Ding, Y., Tang, L., Hla, T., Zeng, R., Li, L., and Wu, D. (2005). Regulation of PTEN by Rho small GTPases. Nat. Cell Biol. *7*, 399–404.

Li, Z., *et al*. (2003). Directional sensing requires G beta gamma-mediated PAK1 and PIX alpha-dependent activation of Cdc42. Cell *114*, 215–227.

Lombardi, M. L., Knecht, D. A., Dembo, M., and Lee, J. (2007). Traction force microscopy in *Dictyostelium* reveals distinct roles for myosin II motor and actin-crosslinking activity in polarized cell movement. J. Cell Sci. *120*, 1624–1634.

Mataraza, J. M., Briggs, M. W., Li, Z., Entwistle, A., Ridley, A. J., and Sacks, D. B. (2003). IQGAP1 promotes cell motility and invasion. J. Biol. Chem. *278*, 41237–41245.

Meili, R., Alonso-Latorre, B., del Alamo, J. C., Firtel, R. A., and Lasheras, J. C. (2010) Myosin II Is essential for the spatiotemporal organization of traction forces during cell motility. Mol. Biol. Cell 21, 405–417.

Meili, R., Ellsworth, C., and Firtel, R. A. (2000). A novel Akt/PKB-related kinase is essential for morphogenesis in *Dictyostelium.* Curr. Biol. *10*, 708–717.

Meili, R., Ellsworth, C., Lee, S., Reddy, T. B., Ma, H., and Firtel, R. A. (1999). Chemoattractant-mediated transient activation and membrane localization of Akt/PKB is required for efficient chemotaxis to cAMP in *Dictyostelium.* EMBO J. *18*, 2092–2105.

Moores, S., Sabry, J., and Spudich, J. (1996). Myosin dynamics in live *Dictyostelium* cells. Proc. Natl. Acad. Sci. USA *93*, 443–446.

Murphy, C., Rock, R., and Spudich, J. (2001a). A myosin II mutation uncouples ATPase activity from motility and shortens step size. Nat. Cell Biol. *3*, 311–315.

Murphy, C. T., Rock, R. S., and Spudich, J. A. (2001b). A myosin II mutation uncouples ATPase activity from motility and shortens step size. Nat. Cell Biol. *3*, 311–315.

Osman, M. A., and Cerione, R. A. (1998). Iqg1p, a yeast homologue of the mammalian IQGAPs, mediates cdc42p effects on the actin cytoskeleton. J. Cell Biol. *142*, 443–455.

Parent, C. A., Blacklock, B. J., Froehlich, W. M., Murphy, D. B., and Devreotes, P. N. (1998). G protein signaling events are activated at the leading edge of chemotactic cells. Cell *95*, 81–91.

Park, K. C., Rivero, F., Meili, R., Lee, S., Apone, F., and Firtel, R. A. (2004). Rac regulation of chemotaxis and morphogenesis in *Dictyostelium.* EMBO J. *23*, 4177–4189.

Pramanik, M. K., Iijima, M., Iwadate, Y., and Yumura, S. (2009). PTEN is a mechanosensing signal transducer for myosin II localization in *Dictyostelium* cells. Genes Cells *14*, 821–834.

Rebstein, P. J., Cardelli, J., Weeks, G., and Spiegelman, G. B. (1997). Mutational analysis of the role of Rap1 in regulating cytoskeletal function in *Dictyostelium.* Exp. Cell Res. *231*, 276–283.

Reichl, E., Ren, Y., Morphew, M., Delannoy, M., Effler, J., Girard, K., Divi, S., Iglesias, P., Kuo, S., and Robinson, D. (2008). Interactions between myosin and actin crosslinkers control cytokinesis contractility dynamics and mechanics. Curr. Biol. *18*, 471–480.

Ren, Y., Effler, J. C., Norstrom, M., Luo, T., Firtel, R. A., Iglesias, P. A., Rock, R. S., and Robinson, D. N. (2009). Mechanosensing through cooperative interactions between myosin II and the actin crosslinker cortexillin I. Curr. Biol. *19*, 1421–1428.

Rubin, H., and Ravid, S. (2002). Polarization of myosin II heavy chain-protein kinase C in chemotaxing *Dictyostelium* cells. J. Biol. Chem. *277*, 36005–36008.

Sallusto, F., and Baggiolini, M. (2008). Chemokines and leukocyte traffic. Nat. Immunol. *9*, 949–952.

Sasaki, A. T., Chun, C., Takeda, K., and Firtel, R. A. (2004). Localized Ras signaling at the leading edge regulates PI3K, cell polarity, and directional cell movement. J. Cell Biol. *167*, 505–518.

Sasaki, A. T., Janetopoulos, C., Lee, S., Charest, P. G., Takeda, K., Sundheimer, L. W., Meili, R., Devreotes, P. N., and Firtel, R. A. (2007). G protein-independent Ras/PI3K/F-actin circuit regulates basic cell motility. J. Cell Biol. *178*, 185–191.

Steimle, P. A., Yumura, S., Cote, G. P., Medley, Q. G., Polyakov, M. V., Leppert, B., and Egelhoff, T. T. (2001). Recruitment of a myosin heavy chain kinase to actin-rich protrusions in *Dictyostelium.* Curr. Biol. *11*, 708–713.

Stites, J., Wessels, D., Uhl, A., Egelhoff, T., Shutt, D., and Soll, D. R. (1998). Phosphorylation of the *Dictyostelium* myosin II heavy chain is necessary for maintaining cellular polarity and suppressing turning during chemotaxis. Cell Motil. Cytoskeleton *39*, 31–51.

Takeda, K., Sasaki, A. T., Ha, H., Seung, H. A., and Firtel, R. A. (2007). Role of phosphatidylinositol 3-kinases in chemotaxis in Dictyostelium. J. Biol. Chem. *282*, 11874–11884.

Tang, L., Franca-Koh, J., Xiong, Y., Chen, M. Y., Long, Y., Bickford, R. M., Knecht, D. A., Iglesias, P. A., and Devreotes, P. N. (2008). tsunami, the *Dictyostelium* homolog of the Fused kinase, is required for polarization and chemotaxis. Genes Dev. *22*, 2278–2290.

Van Haastert, P. J., and Veltman, D. M. (2007). Chemotaxis: navigating by multiple signaling pathways. Sci. STKE *2007*, pe40.

Van Keymeulen, A., Wong, K., Knight, Z. A., Govaerts, C., Hahn, K. M., Shokat, K. M., and Bourne, H. R. (2006). To stabilize neutrophil polarity, PIP3 and Cdc42 augment RhoA activity at the back as well as signals at the front. J. Cell Biol. *174*, 437–445.

Vazquez, F., and Devreotes, P. (2006). Regulation of PTEN function as a PIP3 gatekeeper through membrane interaction. Cell Cycle *5*, 1523–1527.

Wang, N., and Suo, Z. (2005). Long-distance propagation of forces in a cell. Biochem. Biophys. Res. Comm. *328*, 1133–1138.

Weber, I., Gerisch, G., Heizer, C., Murphy, J., Badelt, K., Stock, A., Schwartz, J. M., and Faix, J. (1999). Cytokinesis mediated through the recruitment of cortexillins into the cleavage furrow. EMBO J. *18*, 586–594.

Weiner, O. D., Neilsen, P. O., Prestwich, G. D., Kirschner, M. W., Cantley, L. C., and Bourne, H. R. (2002). A PtdInsP(3)- and Rho GTPase-mediated positive feedback loop regulates neutrophil polarity. Nat. Cell Biol. *4*, 509–513.

Wessels, D., Soll, D. R., Knecht, D., Loomis, W. F., De Lozanne, A., and Spudich, J. (1988). Cell motility and chemotaxis in *Dictyostelium* amebae lacking myosin heavy chain. Dev. Biol. *128*, 164–177.

Wu, D., Asiedu, M., and Wei, Q. (2009). Myosin-interacting guanine exchange factor (MyoGEF) regulates the invasion activity of MDA-MB-231 breast cancer cells through activation of RhoA and RhoC. Oncogene *28*, 2219–2230.

Xu, J., Wang, F., Van Keymeulen, A., Herzmark, P., Straight, A., Kelly, K., Takuwa, Y., Sugimoto, N., Mitchison, T., and Bourne, H. R. (2003). Divergent signals and cytoskeletal assemblies regulate self-organizing polarity in neutrophils. Cell *114*, 201–214.

Xu, X. S., Lee, E., Chen, T., Kuczmarski, E., Chisholm, R. L., and Knecht, D. A. (2001). During multicellular migration, myosin ii serves a structural role independent of its motor function. Dev. Biol. *232*, 255–264.

Yumura, S., and Fukui, Y. (1998). Spatiotemporal dynamics of actin concentration during cytokinesis and locomotion in *Dictyostelium.* J. Cell Sci. *111*, 2097–2108.

Yumura, S., Yoshida, M., Betapudi, V., Licate, L. S., Iwadate, Y., Nagasaki, A., Uyeda, T. Q., and Egelhoff, T. T. (2005). Multiple myosin II heavy chain kinases: roles in filament assembly control and proper cytokinesis in *Dictyostelium.* Mol. Biol. Cell *16*, 4256–4266.

Zhang, S., Charest, P. G., and Firtel, R. A. (2008). Spatiotemporal regulation of Ras activity provides directional sensing. Curr. Biol. *18*, 1587–1593.

SUPPLEMENTAL FIGURES

Supplemental Figure 1. DIAS analysis of chemotaxing wild-type cells. Areas in **green** represent areas of plasma membrane extension compared to the previous frame. Areas in **red** are areas of membrane retraction. Upper panel, no treatment. Lower panel, treatment of cells with 60 μM LY294002 for 20 min before chemotaxis assays. Assay was done in the presence of 60 μM LY294002.

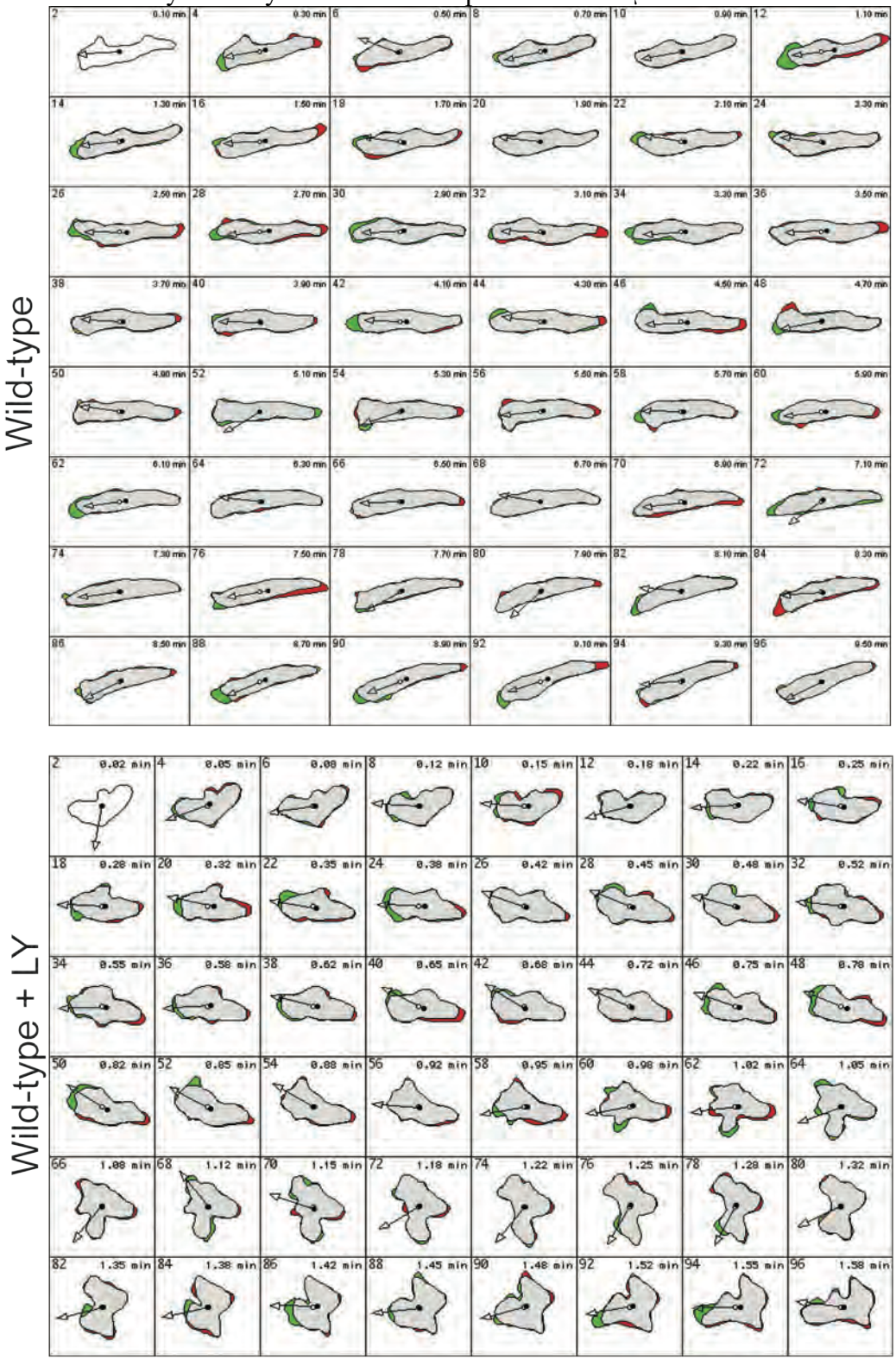

Lee et al, Suppl. Fig. 1

Supplemental Figure 2. DIAS analysis of chemotaxing *mhcA*$^-$ cells. Areas in **green** represent areas of plasma membrane extension compared to the previous frame. Areas in **red** are areas of membrane retraction. Upper panel, no treatment. Lower panel, treatment of cells with 60 μM LY294002 for 20 min before chemotaxis assays. Assay was done in the presence of 60 μM LY294002.

mhcA$^-$

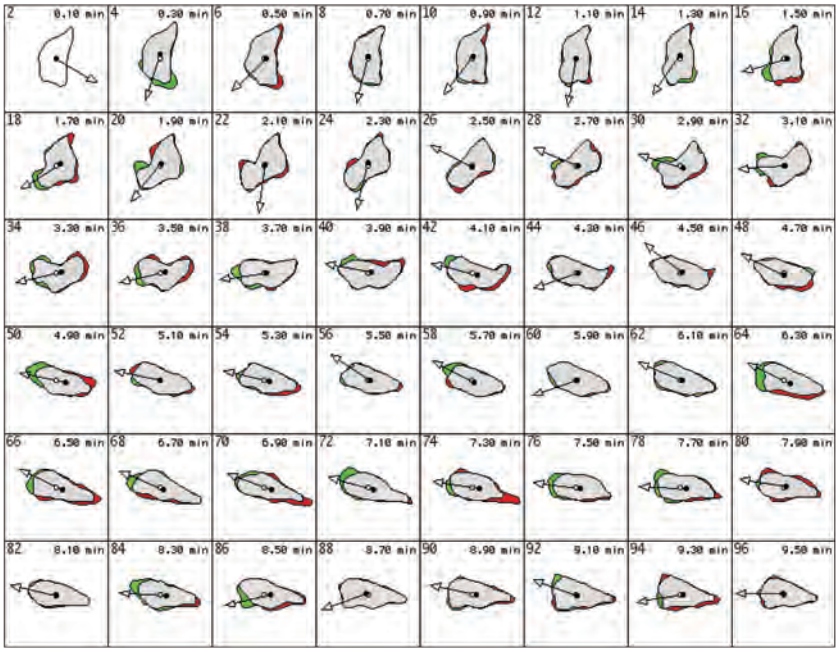

mhcA$^-$+LY

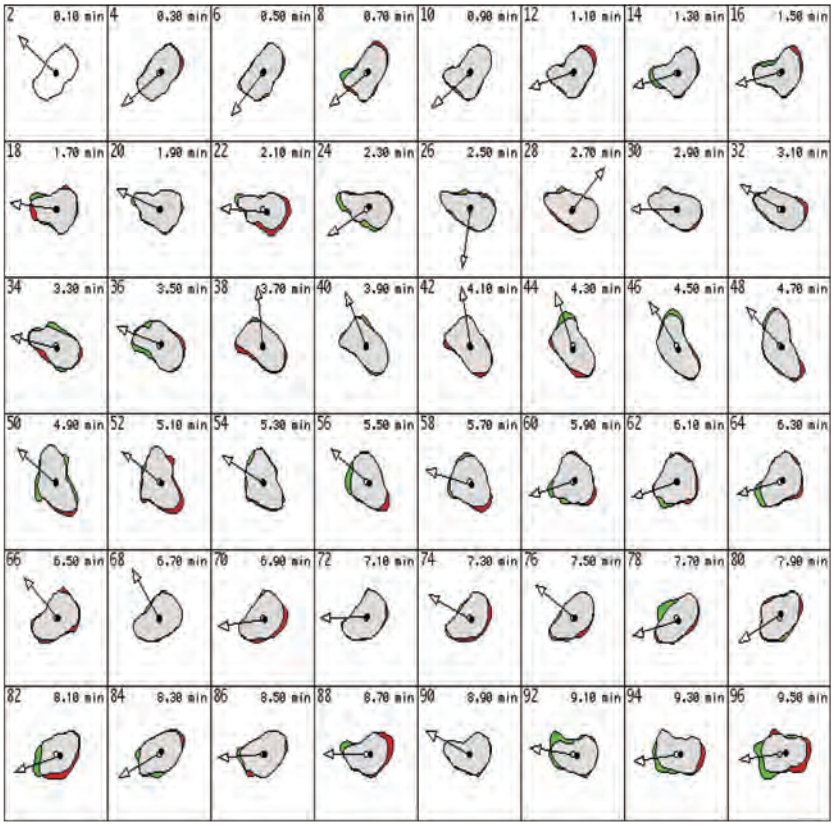

Lee et al, Suppl. Fig. 2

Supplemental Figure 3. Partial list of peptides identified in the mass spectrometry analysis of the myc-IQGAP1 and IQGAP2-containing complex but not found in pull-downs from wild-type control cells. Proteins found in common with the control samples are not shown.

IQGAP1 mass spec

Locus	DDB0191437	DDB019113	DDB0185031	DDB0232236	DDB0214822	DDB0219941	DDB0214823
GENE	iqgap1	ctxA	ctxB	ctxC	rac1A	rac1B	rac1C
# of peptides	50	34	31	7	8	6	4
total of peptides	665	313	264	37	48	9	5
% of coverage	53	68	69	24	35	30	26
M.W.	94925	50505	50460	62233	21572	21676	21550

IQGAP2 mass spec

Locus	DDB191293	DDB0191103	DDB0185031	DDB0214822	DDB0219941	DDB0214823
GENE	iqgap2	ctxA	ctxB	rac1A	rac1B	rac1C
# of peptides	49	34	31	8	6	4
total of peptides	208	73	53	27	18	8
% of coverage	62	68	69	35	30	26
M.W.	98825	50505	50460	21572	21676	21550

Lee et al, Suppl. Fig. 3

Supplemental Figure 4. Co-immunoprecipitation of IQGAP1 and ctx. Cell lysates from cells co-expressing myc-IQGAP1 or myc-IQGAP2 and V5-ctx were immunoprecipitated with anti-myc or anti-V5 antibody and were subsequently probed with either anti-V5 or anti-myc antibody.

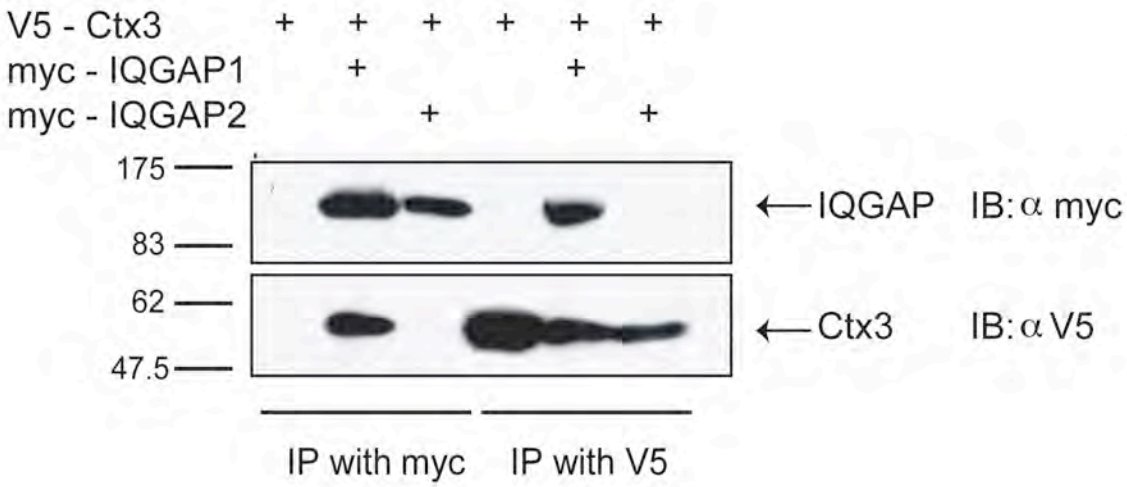

Lee et al, Suppl. Fig. 4

Supplemental Figure 5. GST-Rac1B (wild-type, Q61L, T17N) were incubated with a cell lysate expressing myc-IQGAP1 or myc-IQGAP1^{K273E,K282E}. The products were probed with an anti-myc antibody. Inputs are indicated in the bottom panel.

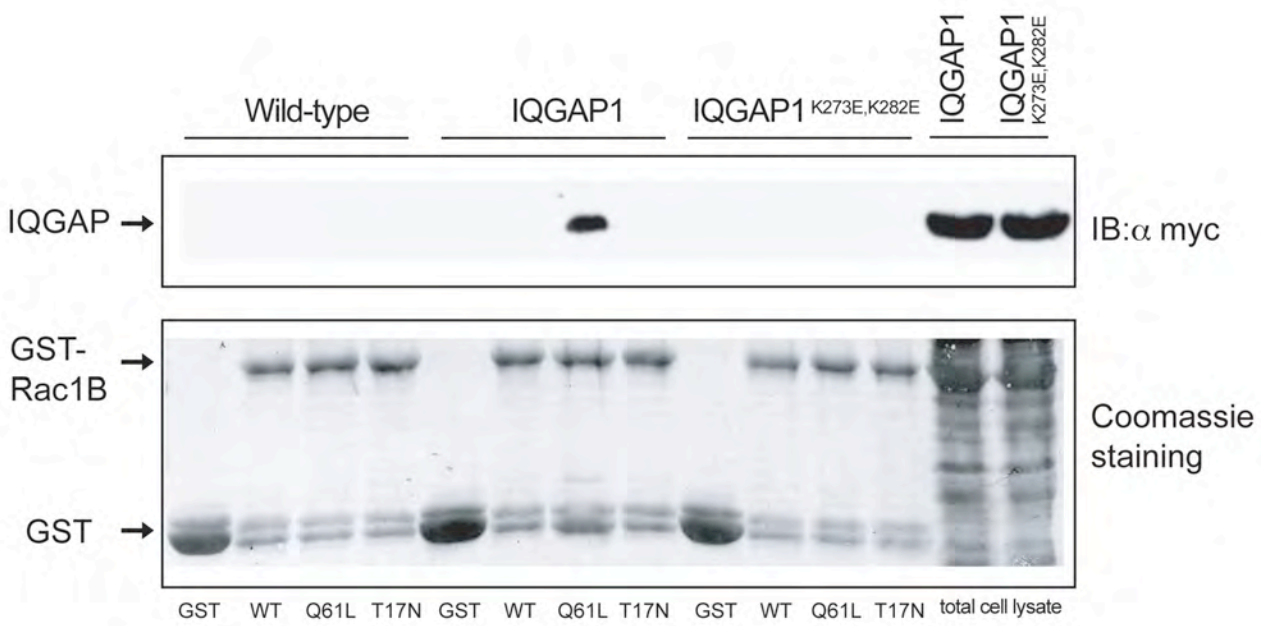

Lee et al, Suppl. Fig. 5

Supplemental Figure 6. Maps and Southern blots for knockout strains. The figure shows the constructs used to create the new knockout strains. Southern blot is of DNA isolated from randomly selected *Dictyostelium* clones. Wild-type control is also shown. The lane numbers refer to individual clones.

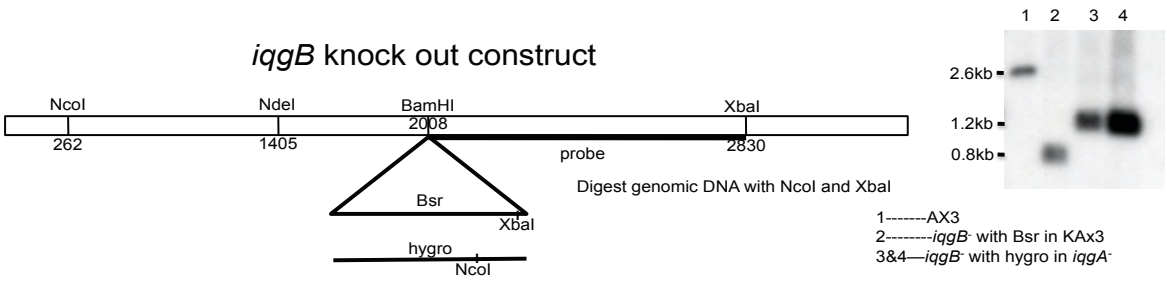

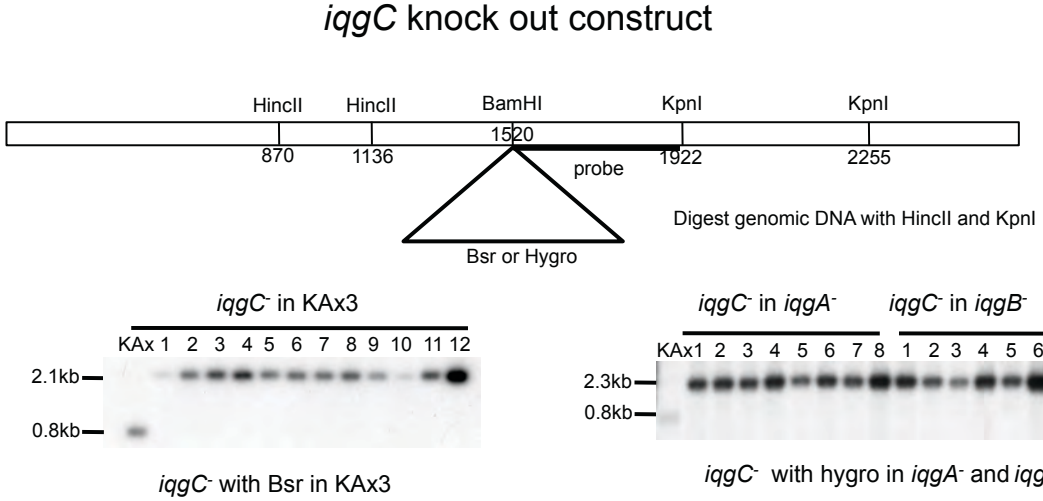

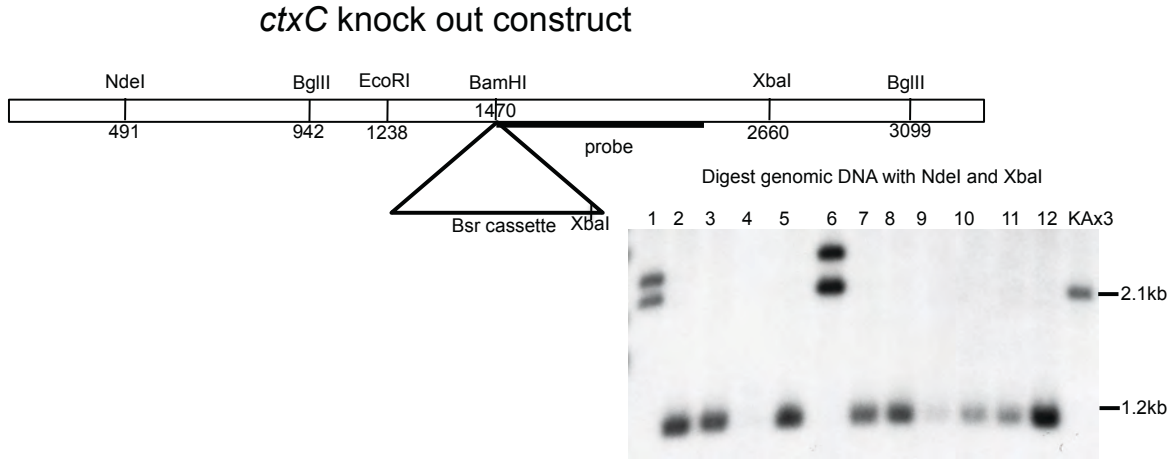

Lee et al, Suppl. Fig. 6